Structures in the active Western Foothills of Southwestern Taiwan: Fault-related folding versus shale tectonics

Hassan Aleem[1], Maryline Le Béon[2], Andrew Tien-Shun Lin[3], Kuo-En Ching[4], Juan I. Soto[5], Kai-Feng Chen[6], and Ngoc-Thao Nguyen[6]

Abstract

Taiwan is an active orogen where a west-verging fold-and-thrust belt deforms a Plio-Pleistocene foreland basin sequence. In southwestern Taiwan, the 3–4 km thick Gutingkeng mudstone, Late Miocene to Early Pleistocene in age, has characteristics similar to mobile shales, such as overpressure conditions and sourcing mud volcanoes. Present uplift rates as fast as 2 cm/year are observed mainly on the footwall of steep thrusts, including the Gutingkeng Fault, which features several mud volcanoes. We integrate surface observations near this fault with regional subsurface data to construct an upper crustal cross section and evaluate the roles of the competing models of fault-related folding and shale tectonics in deforming the region. Field observations indicate steep and well-preserved bedding on the hanging wall and footwall and a wide reverse fault zone with penetrative shearing corresponding to the Gutingkeng Fault. No distinct structure explaining footwall uplift is found in the outcrops. At the cross-section scale, surface geology and subsurface data point to a structural style with fairly narrow anticlines with steep limbs growing above a relatively deep detachment. This geometry is not easily explained using classical fault-related fold models. We infer that folding on the Gutingkeng Fault footwall and in the core of a frontal anticline occurs through layer thickening (pure shear) facilitated by weak mudstone rheology. The increase in pore-fluid pressure under burial and tectonic compression within the fold cores can lead the mudstone to mobilize and undergo plastic flow, causing the inflation of the fold cores. Fold growth, possibly aided by shale tectonics, will have progressively increased the dip of the Gutingkeng thrust, eventually leading to thrust inactivity and uplift mainly occurring on the footwall. Our study area offers a unique opportunity to study an active shale-dominated fold-thrust belt exposed on-land and highlights the importance of combining geodetic observations to investigate ongoing deformations in these settings.

Introduction

Tectonic processes involving mobile shales are collectively called "shale tectonics" (e.g., Vendeville and Jackson, 1992; Soto et al., 2010; Wood, 2010). Shale tectonics is an important problem as it has implications for the petroleum industry and hazard studies. Mobile shale structures consist of mud volcanoes, shale diapirs, and subsurface folds characterized by inflated fold cores (Soto et al., 2021a). The term mobile shale was defined by Morley and Guerin (1996) as "any shales deforming via a combination of ductile deformation and brittle failure in the presence of fluid." This term was previously used by others (e.g., Skeryanc and Kolodny, 1983; Cohen and McClay, 1996). Using soil mechanics concepts, Soto et al. (2021a) redefine mobile shales as "clay-rich sediments or rocks undergoing penetrative, (visco-) plastic deformation at the critical state." Regions with thick mobile shale sequences deforming complexly under brittle and ductile conditions and showing evidence for flow have been studied worldwide (e.g., Morley and Guerin,

[1]Formerly National Central University, Graduate Institute of Applied Geology, Zhongli, Taiwan; National Central University, Carbon Storage and Geothermal Research Center, Zhongli, Taiwan; and presently, Victoria University of Wellington, School of Geography, Environment and Earth Sciences, Wellington, New Zealand. E-mail: hasanaleem2211345@gmail.com.

[2]National Central University, Graduate Institute of Applied Geology, Zhongli, Taiwan; National Central University, Earthquake Disaster and Risk Evaluation and Management Center (E-DREaM), Zhongli, Taiwan; and National Central University, Department of Earth Sciences, Zhongli, Taiwan. E-mail: mlebeon@g.ncu.edu.tw (corresponding author).

[3]National Central University, Carbon Storage and Geothermal Research Center, Zhongli, Taiwan and National Central University, Department of Earth Sciences, Zhongli, Taiwan. E-mail: andrewl@ncu.edu.tw.

[4]National Cheng-Kung University, Department of Geomatics, Tainan, Taiwan. E-mail: jingkuen@mail.ncku.edu.tw.

[5]The University of Texas at Austin, Bureau of Economic Geology, Jackson School of Geosciences, Austin, Texas, USA and On leave of absence from: Granada University, Departamento de Geodinámica, Granada, Spain. E-mail: jsoto@ugr.es; juan.soto@beg.utexas.edu.

[6]National Central University, Graduate Institute of Applied Geology, Zhongli, Taiwan. E-mail: 880324abc@gmail.com; nnthao28@gmail.com.

Manuscript received by the Editor 2 March 2024; revised manuscript received 25 October 2024; published ahead of production 24 December 2024; published online 12 March 2025. This paper appears in *Interpretation*, Vol. 13, No. 2 (May 2025); p. T327–T346, 11 FIGS.
https://doi.org/10.1190/INT-2024-0030.1

1996; Sandal, 1996; Soto et al., 2010; Morley et al., 2017), with insights into their overpressure conditions (e.g., Morley, 1992, 2003; Tingay et al., 2007, 2009, 2013; Morley et al., 2011; Fernández-Ibáñez and Soto, 2017; Tingay, 2017) and structural styles (Morley et al., 1998, 2017, 2018; Hudec and Soto, 2021; Soto and Hudec, 2023). Other processes that could produce shale mobilization are due to hydrofracturing, as extensively documented by Brown (1990), Morley et al. (1998, 2014, 2023), and Morley (2003).

The mobility of shales remains debated. For example, Day-Stirrat et al. (2010) suggest that it is highly unlikely for deep-seated shales to be mobilized and flow even in high-overpressure conditions due to the cementation associated with their chemical compaction. However, in a recent review, Soto et al. (2021a) propose that shales become mobile upon reaching their critical state. Fluid content in shales could increase with burial (due to the diagenetic transformation of clays and organic matter into different types of hydrocarbons), as well as due to compression (including shear-induced or tectonic overpressure; e.g., Yue and Suppe, 2014; Soto et al., 2021b). When the shale peak strength is surpassed, the development of fractures and overpressure conditions will lead to achieving the critical state, at which the previous shale fabric is completely destroyed, and the consolidated sedimentary rock can flow. With this model, it is plausible to have mobile shales with the ability to flow and form inflated fold cores and diapirs under deep burial conditions, as well as fluidized mud forming extrusive mud volcanoes at the surface.

In the southwestern Taiwan fold-and-thrust-belt, rapid compression (−1 μ strain/year) is associated with extremely limited seismicity (Hsu et al., 2009; Ching et al., 2016). This raises questions about the mechanism of the deformation in the upper crust and the mode of the slip of active faults in the region, where the subsurface is dominated by the Gutingkeng mudstone, a significantly thick (3–4 km) Late Miocene to Early Pleistocene clay-rich sequence. This formation is presumably involved in shale tectonic processes, as it has been demonstrated to be a source layer for mud volcanoes (Sun et al., 2010) (Figure 1), indicating overpressured mudstone in the subsurface. Overpressure conditions were also reported

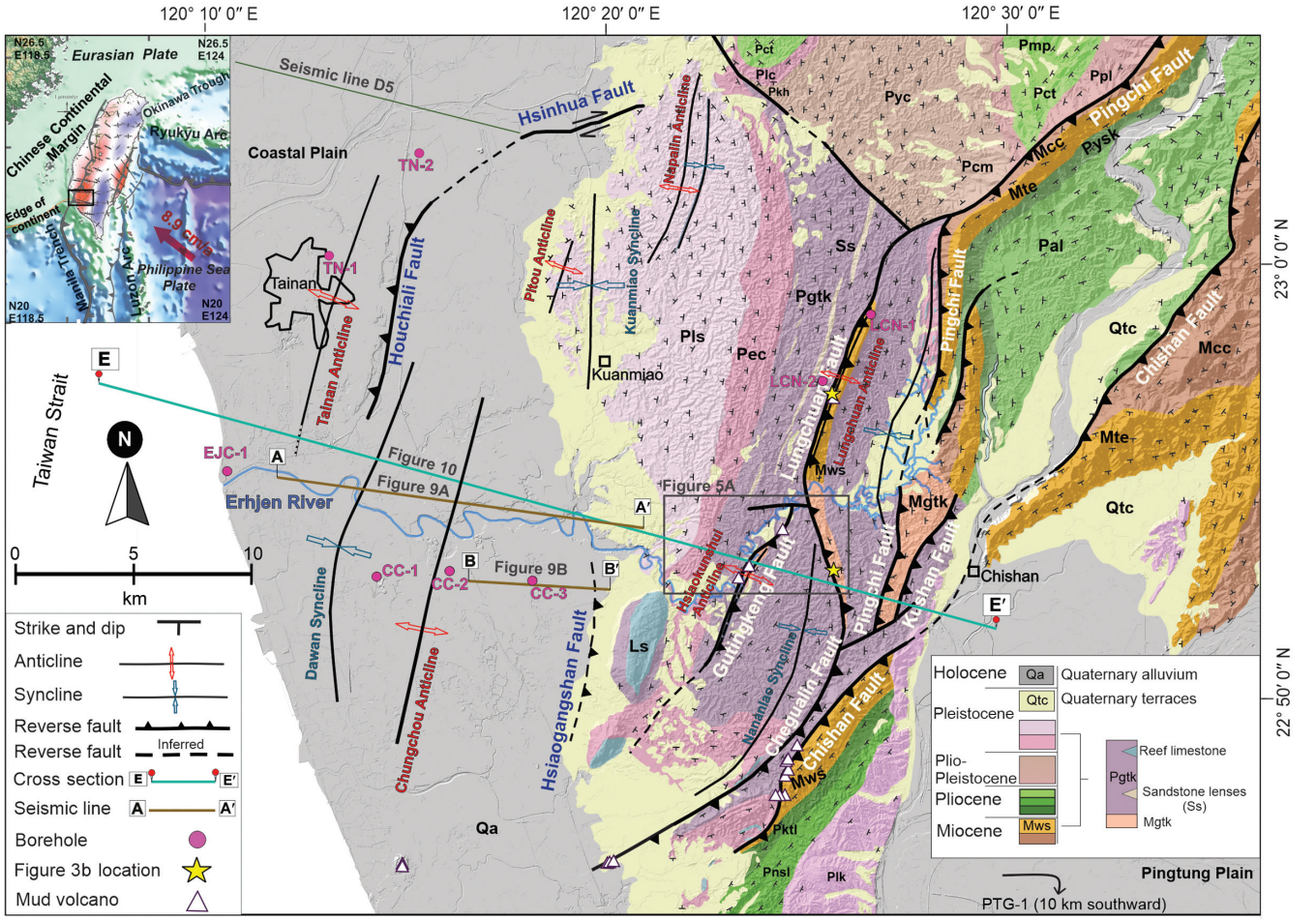

Figure 1. Geologic map of southwestern Taiwan, superimposed on topography (20 m digital earth model [DEM]) (modified after Chinese Petroleum Corporation [CPC] [1989] and Le Béon et al. [2017]). The study area is located within the black rectangle outlined in the inset map. Inset map: the colors indicate the strain rates over Taiwan island (Hsu et al., 2009) with −1 μ strain/year (compression) in red and 1 μ strain/year (extension) in blue. Information about lithostratigraphy is summarized in Figure 3a. Well records are shown in Figure 4.

from deep boreholes within the Gutingkeng Formation and other clay-rich formations of similar age (Yuan et al., 1987). Regionally, mud volcanoes erupt fluidized muddy sediments rich in methane (Chao et al., 2010; Sun et al., 2010). The high Cl content (reflecting the marine origin of the pore water), thermogenic methane, and nannofossil assemblages attest to a deep source, mainly in the Late Miocene to Pleistocene formations (You et al., 2004; Liu et al., 2009; Chao et al., 2010, 2013; Sun et al., 2010). Using seismic reflection profiles offshore, Chen et al. (2014) identify numerous mud volcanoes that occur along the culmination of interpreted mud diapirs and shale-cored anticlines. It was proposed that onshore anticlines are formed similarly and simultaneously to the offshore mud diapirs (Sun and Liu, 1993; Huang, 1995; Liu et al., 1997; Huang et al., 2004; Chuang, 2006; Chen et al., 2020). However, the seismic expression of this thick mudstone sequence in seismic profiles is relatively poor and contains abundant seismic noise and lateral diffractions (e.g., Hsieh, 1972; Huang et al., 2004).

Peculiar ongoing deformation patterns were observed in southwestern Taiwan thanks to Geodesy global navigation satellite system (GNSS), precise leveling, and interferometric synthetic aperture radar (InSAR) line-of-sight velocities), such as aseismic sharp vertical or horizontal deformation gradients and increased deformation rates following regional earthquakes (Pathier et al., 2014; Ching et al., 2016, 2018; Lu et al., 2024). In particular, uplift occurs on the footwall of several west-verging thrust faults, where the Gutingkeng mudstone is involved (Figure 2), whereas the uplifting side of a reverse fault is expected to be its hanging wall (e.g., Fossen, 2016). An example of footwall deformation is seen along the Lungchuan Fault, where interseismic uplift as well as aseismic transient deformation after the Meinong earthquake (2016/02; Mw 6.4) have been documented (Huang et al., 2016; Le Béon et al., 2017; Yi et al., 2023). Le Béon et al. (2017) suggest the activation of a bedding-parallel backthrust within the Gutingkeng mudstone to account for this phenomenon. In addition, subsequent to the Meinong event, minor deformations were noted in the Kuanmiao area, attributed to the aseismic creep on other faults and bending-moment faults activated during shortening and folding within the Gutingkeng mudstone (Le Béon et al., 2017; Yi et al., 2023). Another example of footwall deformation is documented along the Chishan Fault, where rapid geodetic uplift rates were measured and are difficult to reproduce using an elastic dislocation model involving thrusts ramping up from a detachment (Ching et al., 2016). In addition, steep normal shear zones were found on the footwall in the Gutingkeng mudstone, suggesting the need for alternative structural and rheological models. Active mud diapirism was proposed to account for the observed uplift rates. Finally, interseismic uplift was also reported on the footwall of the Gutingkeng Fault (Ching et al., 2016) (Figure 2), corroborated by the Late Holocene river incision rates of 2–2.5 cm/year derived from ^{14}C-dated fluvial terraces of the Erhjen River (Hsieh and Knuepfer, 2001). A doming or anticline structure was proposed to cause the uplift and progressive tilting of the terraces.

In this study, we focus on various contractional structures within the Gutingkeng mudstone in the southwestern Taiwan fold-and-thrust belt. Our main objectives are to understand the structures responsible for the active uplift on the thrust footwalls, focusing on the Gutingkeng Fault, and to evaluate whether shale tectonic concepts can be used to address some of the limitations of the thrust fault-related folding mechanisms. With this intention, we conducted field investigations on the Gutingkeng Fault hanging wall and footwall and generated a regional geologic cross section that integrates observations of active uplift with surface geology and subsurface data, such as the well data and seismic reflection profiles. Determining the geometries of the thrust-related structures and understanding the possible contributions of mobile shales would contribute to the assessment of seismic and surface deformation hazards in the region.

Regional geology and tectonics

Precollision rifting and modern tectonic setting

The formation of the Taiwan orogen is a consequence of the ongoing collision, started in the Late Miocene, between the Luzon Arc situated on the Philippine Sea Plate and the continental margin of Eurasia (e.g., Suppe, 1981; Ho, 1986; Teng, 1990) (see the inset in Figure 1). The orogen is characterized by five tectonostratigraphic zones, oriented north–south and delineated by major faults. These zones, arranged from east to west, include the volcaniclastic Coastal Range, the metamorphic Central Range and Hsuehshan Range, the sedimentary fold-and-thrust belt also called the Western Foothills, and the fluvio-marine Coastal Plain.

Before the Taiwan mountain belt was formed, periods of rifting during the Paleocene-Eocene led to the opening of the South China Sea (Taylor and Hayes, 1983; Lin and Watts, 2002; Teng and Lin, 2004; Yang et al., 2006, 2016), followed by the Oligocene-Miocene rifting episode. In southwestern Taiwan, offshore and onshore, the Paleocene-Eocene rift episode was followed by the Oligocene-Recent postrift subsidence and the development of the Tainan Basin, which consists of northeast to east-northeast horsts and grabens, well-identified by seismic profiles and complemented with borehole information (e.g., Lee et al., 1993; Lin, 2001; Lin et al., 2003; Yang et al., 2016). Rifting was succeeded by collision, marking the onset of foreland sedimentation along the flexed continental margin (Lee et al., 1993; Lin and Watts, 2002).

The horst-and-graben structure extends underneath the Coastal Plain, and the possible continuation of these structures underneath the Western Foothills is a long-lived idea (e.g., Lin and Watts, 2002). A general southeast deepening of the foreland basin is observed from subsurface data (e.g., Covey, 1986; Lin et al., 2003) and lithofacies analysis of the Late-Miocene and Pliocene strata (e.g., Castelltort et al., 2011; Nagel et al., 2013).

Yet, the existence of smaller basins was proposed based on along-strike variations in the lithologies and tectonic structures within the fold-and-thrust belt, which are interpreted to result from the reactivation of preexisting normal faults (e.g., Suppe, 1986; Mouthereau et al., 2006; Álvarez-Marrón et al., 2014; Camanni et al., 2016; Yang et al., 2016; Brown et al., 2017). Brown et al. (2022) confirm this interpretation using a P-wave isovelocity surface of 5.2 km/s as a proxy for the basement-cover interface to interpret several basement highs and lows beneath the Coastal Plain and Western Foothills.

Geologic setting of southwestern Taiwan

Our area of interest in southwestern Taiwan, at the latitude of the Erhjen River (Figure 1), is undergoing an approximately 4 cm/year of westward shortening between the Pingtung Plain and the coastline (Ching et al., 2016, 2018). The fold-and-thrust belt developed on the outer shelf and slope setting of the Eurasian continental margin since the Late Miocene and is characterized by approximately northeast–southwest-striking faults and folds, mainly verging to the west (Mouthereau et al., 2001; Le Béon et al., 2017; Biete et al., 2018). From east to west, the major faults include the Chishan Fault, Lungchuan Fault, Chegualin Fault, and Gutingkeng Fault, which strike N25°–30°E, dip to the southeast, and bring Late Miocene formations on top of the Plio-Pleistocene Gutingkeng mudstone (Figures 1 and 2). To the west, the Hsiaogangshan Fault is understood as a possible blind thrust fault that uplifted the Gutingkeng mudstone and Pleistocene coral reef limestone above the Holocene coastal plain (Gong et al., 1996, 1998; Shyu et al., 2016) (Figure 1). Uplift was proposed to be related to mud diapirism (Sun and Liu, 1993) or a west-verging thrust-related anticline (Lacombe et al., 2004).

In the Coastal Plain, positive gravity anomalies suggest the presence of anticlines (e.g., Lacombe et al., 1999) or mud diapirs, most likely formed by compression (Pan, 1968; Hsieh, 1972; Lo et al., 2023) (Figure 2). Positive anomalies match the subtle topographic highs in the plain, as well as the areas with higher uplift (or lower subsidence) documented by geodetic data (Huang et al., 2006; Ching et al., 2016, 2018) and Holocene uplift rates (Chen and Liu, 2000; Le Béon et al.,

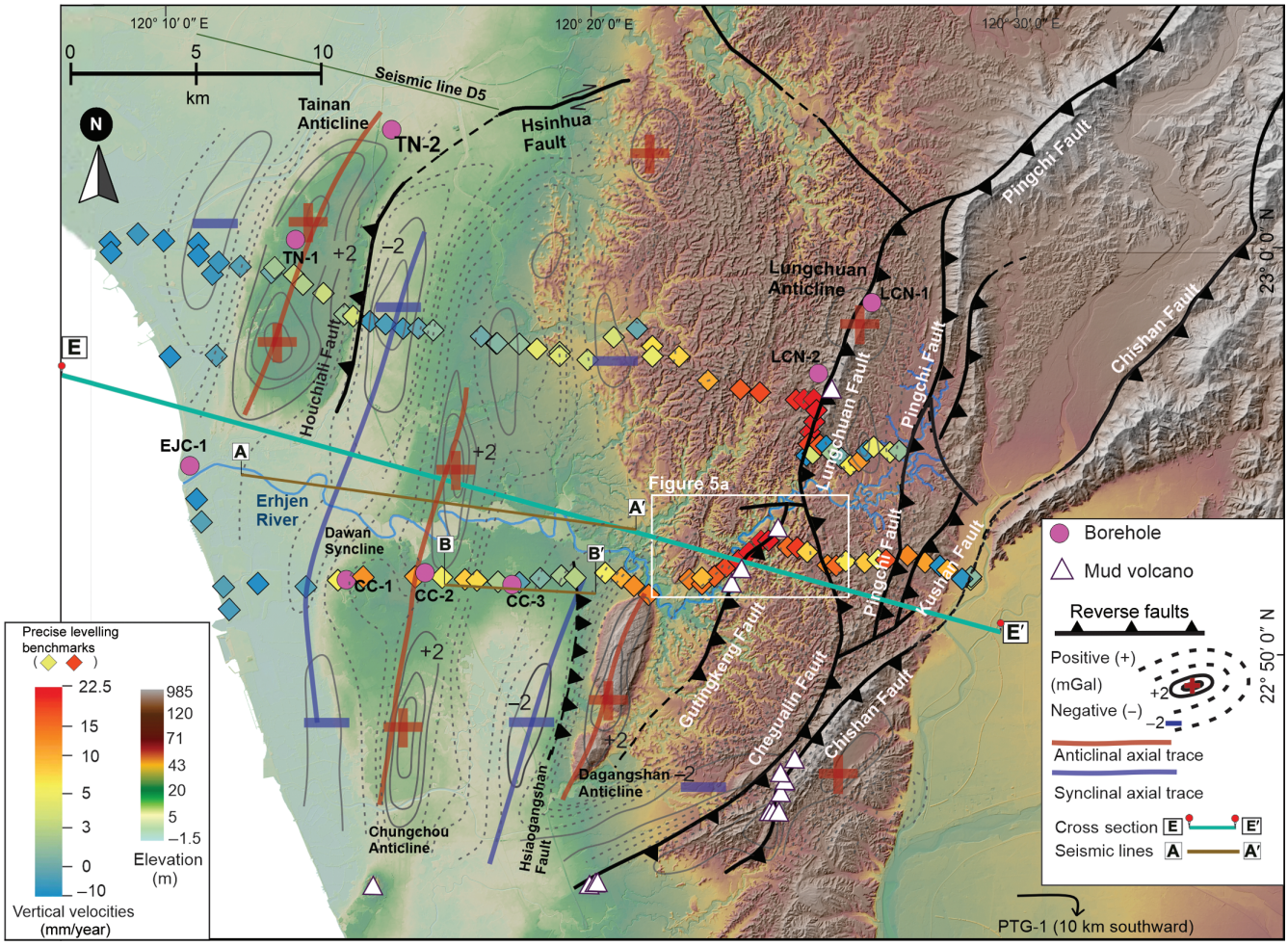

Figure 2. Tectonic map of southwestern Taiwan, including the Bouguer gravity anomaly, corrected for regional gravity effects (contour lines at 0.5 mGal intervals) and modern vertical velocities from precise leveling measurements (2010–2016) (Ching et al., 2018). This information is superimposed on a 20 m DEM. The fold axes in the Coastal Plain are from Hsieh (1972).

2019), demonstrating the activity of these structures. Positive gravity anomalies were also observed offshore across structures interpreted as active mud diapirs based on seismic reflection data (Doo et al., 2015).

Lithostratigraphy

The geologic formations in this region are mainly comprised of mudstone, siltstone, and sandstone and range from the Middle Miocene to the Pleistocene in age, with a Holocene marine and alluvial cover (Figures 1 and 3a). The oldest precollisional Miocene rocks exposed belong to the Changchihkeng Formation (Mcc) (e.g., Lacombe et al., 1999; Lin et al., 2003). The Gutingkeng mudstone (Pgtk and Mgtk) ranges in age from the Late Miocene to the Pleistocene, according to nannofossil age analysis (Chi, 1978; Horng and Shea, 1994; Horng, 2014; Yang et al., 2018). It was deposited in a moderately deepwater marine realm of the upper slope domain of the continental platform (Oinomikado, 1955; Covey, 1986; Brown et al., 2017). In the landscape, it is associated with low-relief badlands. Rock formations in the Chishan area (Figures 1 and 3a), namely the Late Miocene Wushan Formation (Mws), the Pliocene Kaitzuliao Shale (Pktl), and the Nanshihlun Sandstone (Pnsl), are correlated with the Late Miocene and Pliocene Gutingkeng Mudstone (Chi, 1978, 1979). The Late Miocene Wushan Formation has been deposited in a shallow marine setting (Lacombe et al., 1999); however, it has facies variations (shallow marine and deeper marine facies) from north to south on the hanging wall of the Lungchuan Fault (Figure 3b). The Liushuang and Erchungchi Formations represent the uplifted foredeep sediments of marine origin (Covey, 1986). These formations belong to the foreland sequence, are Pleistocene in age, and consist of brackish to fluvial mudstones and sandstones and interbedded shallow-marine shales and sandstones, respectively (Mouthereau et al., 2001). In addition, Pleistocene coral reef limestone hills crop out in a few locations in the Western Foothills (Ho, 1986) (Figure 1).

Data and methods

We compiled previously published data, including borehole information, vintage seismic reflection profiles, gravity data, leveling data, bio and magnetostratigraphy, and surface geology from geologic maps, complemented with data from our field surveys. We also observed mud volcanoes (Chiu et al., 2006; Chen et al., 2014) and confirmed their existence in the vicinity of the Gutingkeng Fault. We used the compiled data set to construct a regional balanced cross section along the transect EE′ (Figure 1).

The compilation of bedding attitudes from previous studies (Chinese Petroleum Corporation [CPC], 1989; Lin et al., 2013) and our own field survey, together with bio and magnetostratigraphy observations (Chi, 1978; Horng and Shea, 1994; Horng, 2014; Yang et al., 2018), allowed us to bracket the location of the Gutingkeng Fault trace, as explained in the "Results" section. Next, we targeted a 350 m long outcrop section at the "pig-farm" locality for a detailed field survey. This section was chosen for its location in the actively uplifting region and on the inferred trace of the Gutingkeng Fault. The length of this outcrop offered the possibility of continuous exposure from the footwall to the hanging wall of the Gutingkeng Fault zone. Hence, we could potentially find structures explaining the Gutingkeng Fault footwall deformation there. We measured the bedding strike and dip and mapped the shear zones. An un-

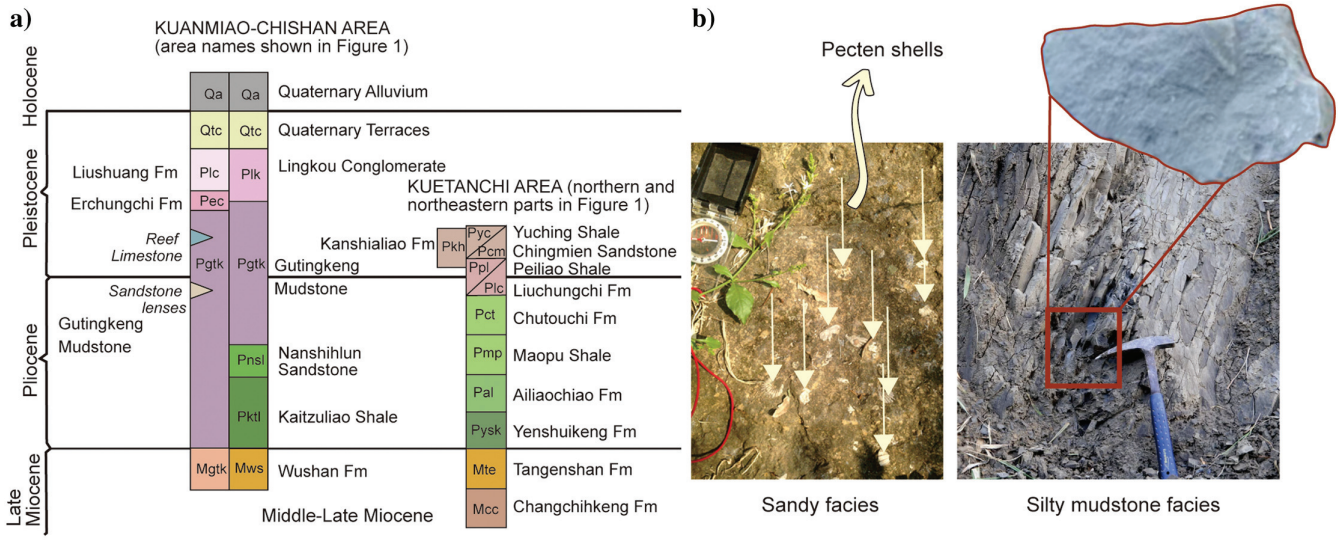

Figure 3. (a) Lithostratigraphy of the study area in southwestern Taiwan (modified after Chinese Petroleum Corporation [CPC] [1989], Horng and Shea [1994], and Yang et al. [2018]). (b) Field photographs (located at the yellow stars in Figure 1) of some of the Late Miocene lithostratigraphic units: the sandy facies with Pecten shells of the Wushan Formation (Mws) (left), located along the Lungchuan Fault north of transect EE′, and the silty mudstone facies of similar age (right), located along EE′ and identified as Mgtk in this study. A close-up view of the silty mudstone sample is also shown.

manned aerial vehicle was used to acquire aerial images to create a basemap for plotting field observations.

To determine the formation thicknesses in the foothills, we used formation boundaries and bedding attitude information from geologic maps and deep boreholes in the Coastal Plain (Figures 1 and 4), including wells CC-1 (true vertical depth [TVD]: 1426 m), CC-2 (TVD: 3964 m), CC-3 (TVD: 4411 m) (Hsieh, 1972), EJC-1 (TVD: 3079 m), and PTG-1 (TVD: 3000 m) (Chiang, 1971). In the absence of surface geologic exposures in the Coastal Plain, the boreholes were projected onto our section line EE′ using the orientation of the fold axis (N15°E) suggested by gravity anomalies (Hsieh, 1972; Lo et al., 2023) (Figure 2). In addition, mud volcanoes located near the Gutingkeng Fault trace were projected to our section transect EE′ along the strike of the Gutingkeng Fault. To reconstruct the thicknesses of the geologic strata beneath the drilled boreholes, we projected the isopachs of the foreland sequence and the depth to the top of the Mesozoic basement (Figure 4 in Lin and Watts [2002] and Figure 2 in Lin et al. [2003]) to our cross section. This data set covers the relatively less deformed region of the western Coastal Plain.

We also used commercial seismic reflection profiles AA′ and BB′ (Shi et al., 2008) to constrain the part of our cross section underneath the Coastal Plain (Figure 1). The seismic profiles are in two-way traveltime and have not been depth converted. The estimation of −1 km depth in AA′ and BB′ is based on seismic line D5 of Le Béon et al. (2019) (Figure 1), which has been depth converted and runs across a similar stratigraphic sequence.

To draw the geologic cross section, we adopted the kink method and the concepts of classical fault-bend folding (e.g., Suppe, 1980), as well as shear fault-related folding and detachment folding (e.g., Shaw et al., 2005). Faults identified as bedding parallel based on geologic maps are extrapolated to the subsurface with the same orientation as surface bedding. Construction using the kink method ensures that each dip measurement represents a zone with a constant dip value. The kinks are useful for understanding the trajectory and displacement of thrust faults at depth (Suppe and Chang, 1983) and are particularly emphasized in the Western Foothills part of the cross section, whereas folds involving basal shear are drawn using curved lines to reflect progressive layer thickening (e.g., Brandes and Tanner, 2014).

Restoring the geologic cross section was accomplished manually by unfolding the lines within the layers considered to have a preserved thickness and by unfolding areas of thickened units (e.g., Fossen, 2016). Restoration was performed toward the hinterland in reference to the nondeformed western tip of the transect. All displacements are considered within the plane of the transect. Changes in volume during shortening have not been considered.

Observations of interseismic uplift come from precise leveling surveys performed yearly since 2003 along several lines extending from the Coastal Plain into the Western Foothills (Ching et al., 2016, 2018). Velocities are integrated with the continuous GNSS velocities and given with reference to the GNSS station S01R, located on Penghu Island in the Taiwan Strait. We analyzed vertical velocity data obtained from 87 measurement benchmarks from 2010 to 2016 (Figure 2). For benchmarks located near the Gutingkeng Fault, we projected

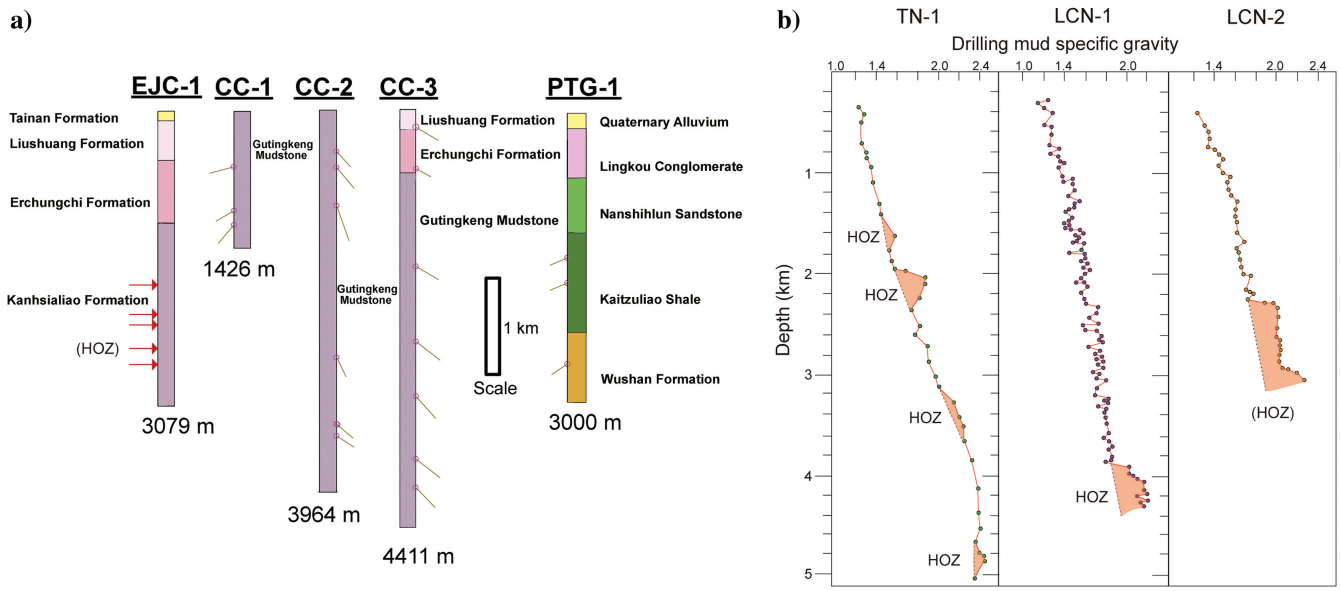

Figure 4. (a) Lithologic logs from various boreholes in southwestern Taiwan (modified after Chiang [1971] and Hsieh [1972]) (see locations in Figures 1 and 2), including bedding dips measured along the wells (the dip orientation is unknown). The red arrows along EJC-1 indicate the depths at which mud flow outs were observed. The age and characteristics of these formations are described in Figure 3. (b) Boreholes showing overpressure conditions (high overpressure zone [HOZ]; highlighted in pink) based on the variations in drilling mud specific gravity (modified after Yuan et al., 1987).

vertical velocities along the fault strike to present the evolution of tectonic uplift across the fault.

Results

General structure and active deformation across the Gutingkeng Fault

The Gutingkeng Fault brings the Late Miocene Gutingkeng mudstone (Mgtk) on top of the Pleistocene Gutingkeng mudstone (Pgtk) (Figures 3 and 5) (Chi, 1978; Horng and Shea, 1994; Horng, 2014; Yang et al., 2018). The hanging wall is folded along the Hsiaogunshui Anticline, which extends only along the central part of the Gutingkeng Fault (Figure 5a). Bedding strike and dip observations are consistent and well-preserved in the region on the hanging wall, with the Nananlao Syncline, and on the footwall, with the west-dipping strata progressively steepening eastward (Figures 1 and 5a).

It is important to note that the exact trace of the Gutingkeng Fault is not certain. Nannostratigraphic ages (Chi, 1978; Horng and Shea, 1994; Horng, 2014; Yang et al., 2018) (Figure 5a) allow us to bracket the fault trace location within 50–100 m along its central part, where the most constraints are available. In addition, identifying the structural characteristics of the hanging wall and footwall enables the extrapolation of the fault trace based on bedding attitudes where age constraints are limited. For instance, northeast of the Hsiaogunshui Anticline, the hanging wall displays a normal sequence of southeast-dipping mudstone, whereas, on the footwall side, the sequence dips west-northwest. Using these constraints, the location of the Gutingkeng Fault trace can be inferred within a 100–150 m wide

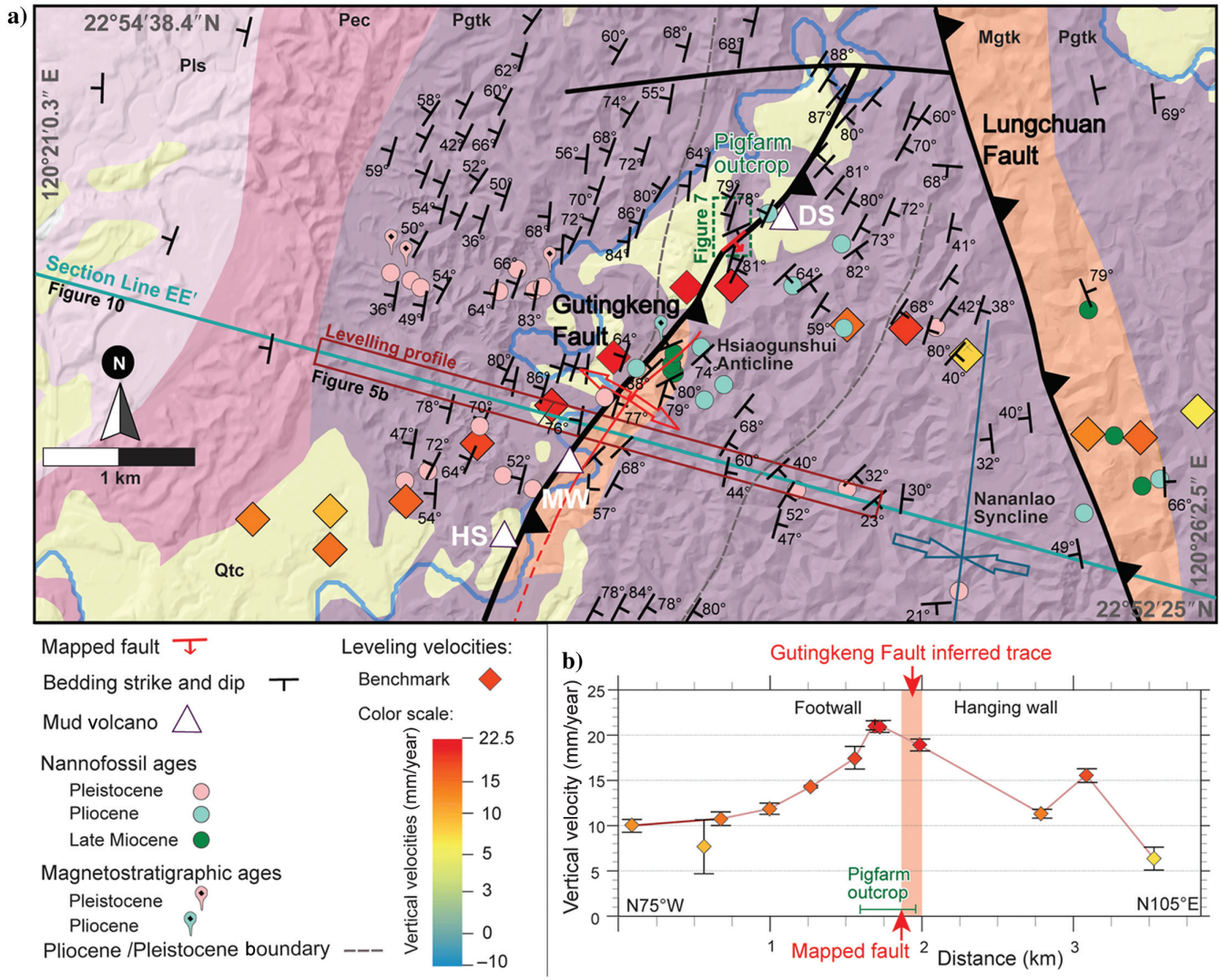

Figure 5. (a) The map of the Gutingkeng Fault featuring bedding details, nannofossil ages (Chi, 1978; Horng and Shea, 1994; Horng, 2014; Yang et al., 2018), and precise leveling observations (Ching et al., 2018). The dotted rectangle marks the position of the pigfarm outcrop detailed in Figure 7. Capital initials stand for mud volcanoes: DS for Dagunshui, HS for Hsiaogunshui, and MW for Moon World. Black initials refer to formations, as indicated in Figure 3a. (b) Leveling profile and observed vertical velocity gradient across the Gutingkeng Fault.

band up to the latitude of the Dagunshui mud volcano (Figure 5a). Establishing the range of possible locations for the inferred fault trace is essential for selecting outcrops to investigate and for interpreting the mud volcanoes location of mud volcanoes and leveling data.

Three active mud volcanoes have been reported in the Gutingkeng Fault area, namely the Dagunshui, Hsiaogunshui, and Moon World (Figures 5a and 6). They can be classified as class-3 mud volcanoes (sensu Alizadeh et al., 2015), representing those that emit low-viscosity mud with no intense gas bursts associated. All of them are located within the narrow band of 100–150 m of the inferred fault trace.

Along the leveling transect in Figure 5b, the inferred Gutingkeng Fault trace is located between 1.9 and 2.0 km. Precise leveling measurements indicate a notable eastward increase in the uplift rate on the footwall, with values of 11.9 ± 0.5 mm/year 0.8 km west of the fault and rapidly increasing to 21.1 ± 0.6 mm/year near the fault. The uplift rate remains high at 18.7 ± 0.6 mm/year 0.1 km into the hanging wall and decreases to 11.1 ± 0.5 mm/year 1 km east of the fault. The high uplift zone is at least 0.9 km wide in the direction perpendicular to the strike of the fault. Combined with the InSAR line-of-sight velocities (Pathier et al., 2014), these observations suggest that uplift affects a wider zone in the footwall compared to the hanging wall.

Structural analysis of the pigfarm outcrop

In the field, we have inspected the surface geology at the pigfarm outcrop (see the location in Figure 5a), an elongated badland slope with nearly continuous exposure, subperpendicular to geologic structures, and situated at the inferred location of the Gutingkeng Fault (as explained in the previous subsection). In this locality, we have carefully studied bedding attitudes and structures associated with the fault zone while also conducting a structural analysis of the observations to evaluate the fault kinematics.

Our observations at the northern part of the outcrop show well-preserved strata with consistent bedding attitudes with steep dips to the northwest (76°–90°) (Figure 7), similar to the bedding attitudes at a wider scale on the footwall (Figure 5a). To the south of this dip domain, several brittle shear zones with variable orientations were observed. We describe the observations made in three areas: the shear zones with southeast-dipping shear planes in zone A, the shear zones with west-dipping shear planes in zone B, and the interaction zone between the southeast-dipping shear planes and the west-dipping shear planes in zone C. In all the cases, the shear zones are characterized by discrete fault surfaces, forming a dense, anastomosing network of black bands and recognized as a product of faulting and shearing in the mudstones (e.g., Vrolijk and Van der Pluijm, 1999; Casciello et al., 2004; Huang, 2015; Jhuang, 2023). We have not been able to find kinematic indicators in the shear zones, such as slickenlines or S-C structures. Because the outcrop offers nearly continuous observations, we assume that all the fault planes represent principal deformation features such as Y fractures (i.e., parallel to the main fault zone), although some of them could be R or P shears forming a small angle with the fault zone.

In zone A (Figure 8a), we observed two shear zones and minor faults. The upper shear zone is oriented at 080°/51°S and identified as the major one as it brought muddier facies on top of siltier facies, hence suggesting significant offset across the shear plane. The silty beds below the major shear zone are slightly offset across a secondary black shear zone oriented at 068°/51°S and a series of southeast-dipping minor faults. The apparent offsets of the top blocks are all to the right. This observation led us to interpret this shear zone as a reverse fault zone, considering that the slip along the major shear plane and secondary plane occurred simultaneously.

In zone B, our observations revealed a continuous west-dipping shear plane (Figure 8b) across which a sandstone bed has been displaced by 0.5 m, with the top block toward the right (Figure 8c). Using stereographic analysis of the displaced sandstone bed (258°/70°N) and the shear plane (170°/56°W) (Figure 8d), we can deduct that any slip vector from the right-lateral strike slip to reverse can lead to the present configuration, hence reverse faulting is a possible solution.

In zone C, we observe a southeast-dipping shear plane that crosscuts a west-dipping shear plane (Figure 8e) and offsets it by approximately 3 m. This offset indicates a reverse movement across the southeast-dipping shear plane. The west-dipping shear plane observed in zone C is continuous southward as far as we could observe and is possibly the same as in zone B. However, the southeast-dipping shear plane in zone C might represent the hanging wall deformation of the main southeast-dipping reverse fault identified in zone A.

To summarize our findings, we have identified a prominent southeast-dipping shear zone that exhibits reverse

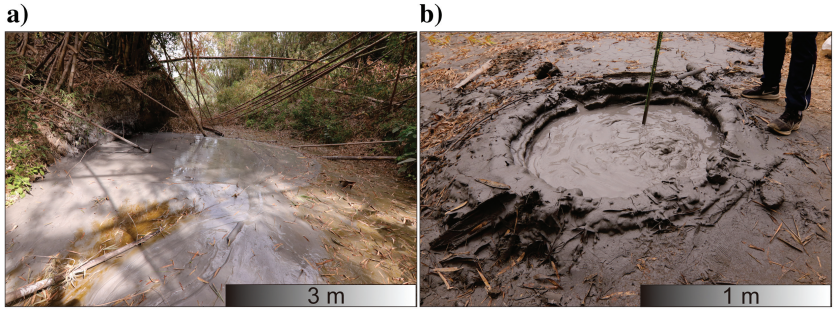

Figure 6. Field photographs of the (a) Moon World and (b) Hsiaogunshui mud volcanoes with a mud pool or salse (sensu Hovland et al., 1997) with low-viscosity mud fluid and methane oozing out. The locations are shown in Figure 5a.

displacement, likely representing the Gutingkeng Fault or the lower part of its fault zone. On the hanging wall of this fault, a west-dipping reverse fault was observed, possibly indicative of synchronous deformation. However, the precise leveling data (Figure 5b) indicate a broad zone of active uplift of up to 22 mm/year, mainly focused on the footwall side of the Gutingkeng Fault, suggesting that the southeast-dipping reverse fault we mapped might not currently be active. On the footwall side, the observed bedding is well preserved, with consistent orientations, even in the vicinity of the fault. At the scale of this 350 m long outcrop section, no distinct geologic structure indicative of a greater uplift on the northwest side compared to the southeast was observed. Nevertheless, steeply dipping beds indicate folding, which could be responsible for the footwall uplift due to a larger-scale structure. Further explanation of the potential structures and causes of folding will be described based on the geologic cross-section EE′ presented hereafter.

The upper crustal structure along the transect EE′

We have built a balanced cross section along the transect EE′ oriented N75°W, which is perpendicular to most geologic structures (see the location in Figure 1). The cross section integrates our field observations, surface geology (Figures 1 and 5a), deep borehole data (Figure 4), and, in the central domain, our interpretation of seismic lines AA′ and BB′ (Figure 9). The resulting geologic cross section and restoration are shown in Figure 10. Our cross section is generated based on the principles of fault-related folding; the possible roles of shale tectonic processes will be assessed in the "Discussion" section. Based on the contrasted structural styles in the foothills and beneath the Coastal Plain, we present our cross-section in two parts, starting from the foothills part.

Structural interpretation east of the Gutingkeng Fault

On the geologic map (Figure 1), the hanging walls of the Gutingkeng and Lungchuan Faults have thrust-related anticlines with the Late Miocene strata along the fold axes. Hence, these faults have hanging-wall cutoffs in the near surface and may root along the Late Miocene or older formations. The Pingchi Fault cross cuts the Late Miocene Gutingkeng Formation (Mgtk) at the surface along transect EE′. Toward the north, it is a bedding-parallel fault (as the hanging wall bedding strikes and stratigraphic contacts are parallel to the fault trace) and exposes the older Miocene Changchihkeng Formation (Mcc) so that it may carry the Mcc Formation in the subsurface at the latitude of EE′. The Chishan Fault is a bedding-parallel fault that exposes the Late Miocene Wushan Formation (Mws) southwest of EE′ and the age-equivalent Tangenshan Formation (Mte) northeast of EE′. The hanging wall geology is also constrained by the PTG-1 borehole, with the top of Wushan at a depth of 2395 m (Chiang, 1971) (Figure 4a) in the Pingtung Plain south of EE′ (Figure 1). Because the east tip of EE′ lies a few kilometers south of

Figure 7. The orthoimage of the pigfarm outcrop with attitudes of bedding and shear planes shown in black and red, respectively. See the location in Figure 5a. Field photographs of zone A are shown in Figure 8a, zone B in Figure 8b–8d, and zone C in Figure 8e.

bedrock outcrops that depict a south-plunging syncline, the top of Wushan is likely a bit shallower along EE′ than at PTG-1. Each thrust sheet displays a wide syncline, either along EE′ or to the north (Figure 1), which provides constraints on the depth at which these faults would flatten.

Based on these inferences, the eastern part of the cross section (Figure 10a) is drawn, accounting for the westward propagation of deformation and using the concept of imbricate structures (Suppe, 1980). A steep Gutingkeng Fault is drawn to flatten on a shallow 3 km detachment at the base of the Late Miocene Gutingkeng (Mgtk) Formation. Because the detachment depth at the base of the Gutingkeng mudstone is shallower than in the western part of the cross section, we proposed a deeper detachment at a depth of approximately 8 km (as proposed in Huang et al., 2004) that ramps up to the Mgtk, is responsible for the growth of a fault-bend fold affecting the Miocene strata (Figure 10a), and contributes to the steepening of the thrust sheets located on top of it, making the upper detachment shallower.

A noticeable difference in the lithology of the Late Miocene formations is illustrated with different shades of orange in Figure 1. In the northern parts of the Lungchuan and Pingchi Faults, as well as along the Chishan Fault south of EE′, the Late Miocene Wushan Formation (Mws) consists of thick sandstone beds, occasionally with Pecten shells (Figure 3b, left side) and standing out in the landscape, most likely due to differential erosion. In contrast, along EE′, the southern Lungchuan Fault, the southern Pingchi Fault, and the Gutingkeng Fault exhumed Late Miocene strata that comprise silty mudstone facies looking very similar to the Gutingkeng mudstone (Figure 3b, right side), and which we classified as Mgtk (Figures 1 and 3). These observations suggest the presence of a former basin, called the "Gutingkeng Basin," represented by the deeper-marine mudstone facies and surrounded by shallow-marine areas represented by the Mws sandstones. It could consist of a half-graben, controlled by a northwest-dipping normal fault at the southeastern edge of the basin, located approximately along the Chishan Fault, or it could be controlled by two bounding normal faults, a northwest-dipping fault along the Chishan Fault and a southeast-dipping fault, oriented N75°W and located at the intersection between the Lungchuan and Gutingkeng Faults. The existence of this basin is compatible with the overall structure of the normal fault systems along the passive margin (e.g., Yang et al., 2016) and its probable extension underneath this part of the mountain belt (e.g., Brown et al., 2022). We favored the half-graben alternative as it looked more convincing during the restoration of the cross section (Figure 10b). After restoration, the eastern edge of the basin would match the eastern edge of the Pingtung Basement Low (Brown et al., 2022).

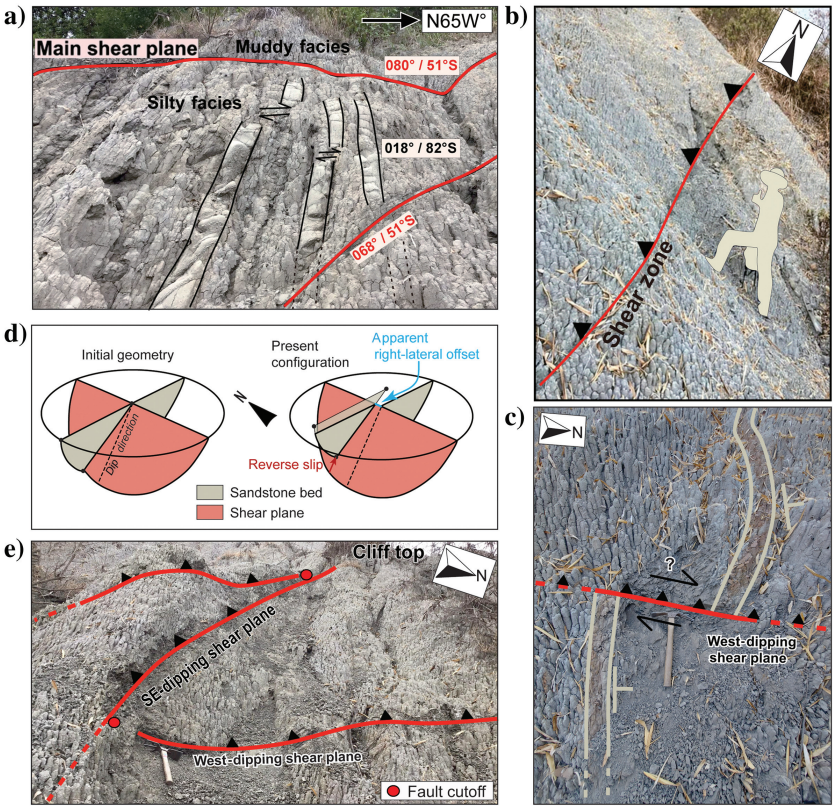

Figure 8. Field observations at the pigfarm outcrop (see the location in Figure 7). (a) The southeast-dipping shear zone located in zone A. This photo is taken while standing on a steep cliff, looking up. (b) The west-dipping shear zone displacing a sandstone bed in zone B. (c) Overview of the west-dipping shear zone in zone B. (d) A 3D stereographic representation schematizing observations made in (b) and (c). The shear plane dip direction is indicated by a dashed line. The right-hand sketch shows that a reverse displacement of the hanging wall bed can explain an apparent right-lateral offset at the surface. (e) A southeast-dipping shear plane cutting and offsetting, with a reverse slip sense, the west-dipping shear plane in zone C. This photo is captured from a steep cliff perspective, looking upward.

Structural interpretation west of the Gutingkeng Fault

To the west of the Gutingkeng Fault, surface geology in the foothills and borehole information in the Coastal Plain (Figure 4a) constrain a significant increase in the thickness of the Gutingkeng mudstone, reaching 3000 m in the syncline east of well CC-3 (Figure 10a). On the footwall of the Gutingkeng Fault, bedding dips gradually steepen toward the east as part of the deeper fold forelimb. The steeper dips are interpreted as a footwall syncline, likely a relic of the initial thrust development as a fault-propagation fold.

We have interpreted two seismic profiles across the Chungchou Anticline in the central domain of the cross-section (Figure 9). The colored reflections probably represent the Erchungchi and Liushuang Formations according to their reflectivity. Their position is also in agreement with our depth conversion estimate (see the red marks in Figure 9). These reflections show growth strata with a progressive fanning upward geometry on the fold's east limb and their onlapping geometry on the west limb. Both geometries indicate that the shortening rates were larger than the sedimentation rates, in particular for the west limb (e.g., Shaw et al., 2005). The asymmetric growth strata point to a fault-related fold (Lacombe et al., 2004) with a west vergence. The progressive increase in the dip of the reflections with depth suggests a shear fault-related folding mechanism characterized by the thickening of a basal layer and a fold limb rotation mechanism. A fault-propagation fold model (e.g., Poblet and McClay, 1996; Poblet, 2011) is proposed as a possible explanation for this geometry. Below the growth strata, the chaotic seismic reflections are compatible with a homogeneous shale sequence, possibly with an intense deformation, which would correspond to the Gutingkeng mudstone. This is consistent with observations in various basins worldwide, where mudstones often present chaotic seismic facies in seismic reflection profiles (e.g., Soto et al., 2021b).

To the west of CC-1, we used thickness constraints from Lin et al. (2003) and Lin and Watts (2002) to draw the foreland and basement units and interpret the basement structures. The base of the foreland sequence, delineated by the top of the Changchihkeng Formation (Mcc), varies slightly from −5500 to −6000 m in depth. We infer this contact to be a detachment level. The depth to the top of the Mesozoic basement is relatively shallow (−6400 to −7000 m) beneath the western part of the Coastal Plain, deepening to 8–10 km toward the southeast (Brown et al., 2022).

Discussion

Mud volcanism near the Gutingkeng Fault

The three active mud volcanoes are located within the narrow band of the inferred trace of the Gutingkeng Fault (Figure 5a), potentially indicating fluid migration through fractures in the fault zone, in agreement, for example, with the proposition of Soto and Hudec (2023). However, the Hsiaogunshui Anticline axis is also located very close. The crest of anticlines generally has extensional fractures that could also act as pathways for fluids to erupt at the surface, in accordance with Bonini (2007) and Mazzini and Etiope (2017). However, the existence of such faults along the crest of the Hsiaogunshui Anticline has not been documented yet. Overpressure is a fundamental condition whether the mud volcano erupts through the crest of the anticline or through a fault zone (see the recent discussion in Soto and Hudec, 2023). Mobile shale systems are often linked to the presence of fluid escape features, for example, mud volcanoes that may, in turn, represent indirect indicators of overpressure conditions in the source layer (e.g., Morley et al., 2011).

Previous studies of the composition of the sediment and fluids of these three mud volcanoes demonstrated the deep origin of their source. The elevated Cl content and the isotopic composition of deuterium and oxygen in the water suggest an origin from ancient seawater,

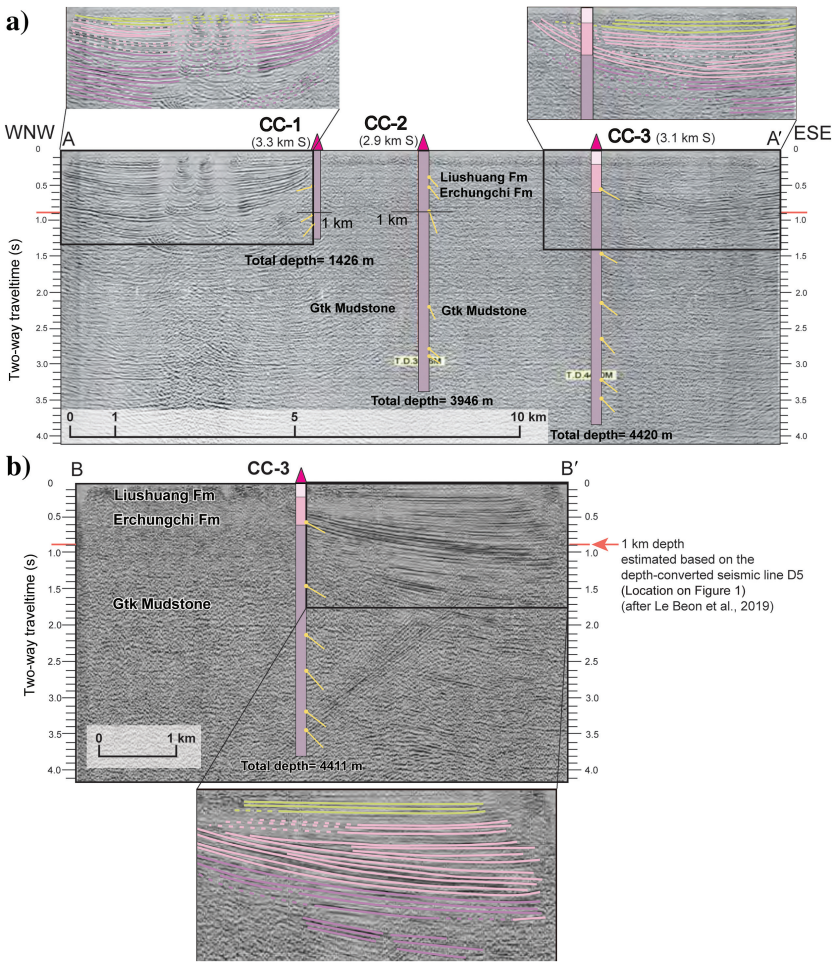

Figure 9. Seismic reflection profiles (a) AA′ and (b) BB′ (modified after Shi et al., 2008) (see the location in Figures 1 and 2), noninterpreted and including our interpretation of the growth strata. The vertical scale for the well data is by depth, whereas the seismic lines are in two-way traveltime (in s), with a 1 km depth roughly equivalent to 0.9 s by analogy with Le Béon et al. (2019). The parentheses following the borehole names indicate the distance and direction between the borehole and the seismic line.

with clay-dehydration involved (You et al., 2004; Liu et al., 2009; Chao et al., 2013). Sun et al. (2010) analyze the composition of the extruded material at four mud volcanoes near the Gutingkeng and Lungchuan Faults. Although the specific mud volcanoes investigated are not clearly identified, the available information shows that they all share similar characteristics: the extruded material contains nannofossil assemblages that are equivalent to the Late Pliocene to Pleistocene age of the Gutingkeng Formation, as well as a mixture of hydrocarbons with biogenic and early maturity thermogenic methane, which are also consistent with the Gutingkeng Formation. Nevertheless, the rocks in the immediate hanging wall of the fault and along the anticline axis are Late Miocene in age. Therefore, we suggest that these mud volcanoes formed from a relatively shallow fluid source in the footwall at a depth of 2 km or less, according to our cross section (Figure 10a). The fluids would more likely use the Gutingkeng thrust as a pathway, yet potential fractures along the anticline axis cannot be excluded due to the proximity between the thrust trace and the anticline axis. The source of these mud volcanoes is shallower and younger than that of other mud volcanoes in the region, for which deeper-sourced fluids would originate from the Middle to Late Miocene formations (Sun et al., 2010).

Evidence and implications of overpressure conditions

The recognition of high-overpressure zones is critical because it is one of the major characteristics of mobile shales (e.g., Soto et al., 2021a). In addition to the presence of mud volcanoes, several boreholes in southwestern Taiwan were reported to have sudden increases in fluid pressure at various depths within the Gutingkeng mudstones. The use of drilling mud of different densities in well operations can be used as an indirect indicator of the conditions in the drilled formation, with drilling mud specific gravity values above 1.45 representing abnormal formation pressure (Chain, 1967). For example, in borehole TN-1, elevated pressure levels have been observed at depths of 1.5, 2.1, 3.5, and 5 km (Figure 4b) (Yuan et al., 1987). In EJC-1, mud flow outs occurred several times at depths ranging from 1.81 to 2.63 km. In the Western Foothills, LCN-1 and LCN-2 exhibit singular but extensive high-pressure zones at depths of 4 and 2.3 km, respectively (Figure 4b) (Yuan et al., 1987). Notably, the high-pressure zone in LCN-2 appears broader and at a shallower depth compared with that in LCN-1. The presence of overpressure at various depths in the Coastal Plain and Western Foothills may be related to local lithologic, stratigraphic, or tectonic conditions.

The inferred role of mobile shales in the fold-and-thrust belt

The presence of a thick mudstone formation characterized by overpressure conditions is evidenced from borehole information (e.g., Yuan et al., 1987) and supported by the presence of mud volcanoes. These are conditions related to mobile shale systems. In the following, we discuss the relations between the geometry of the structures, constructed based on fault-related folding principles, and the active uplift observed from geodesy. We then assess where and how shale tectonics could help to explain some of the observations and singular characteristics of the structures depicted in the cross section (Figure 10a).

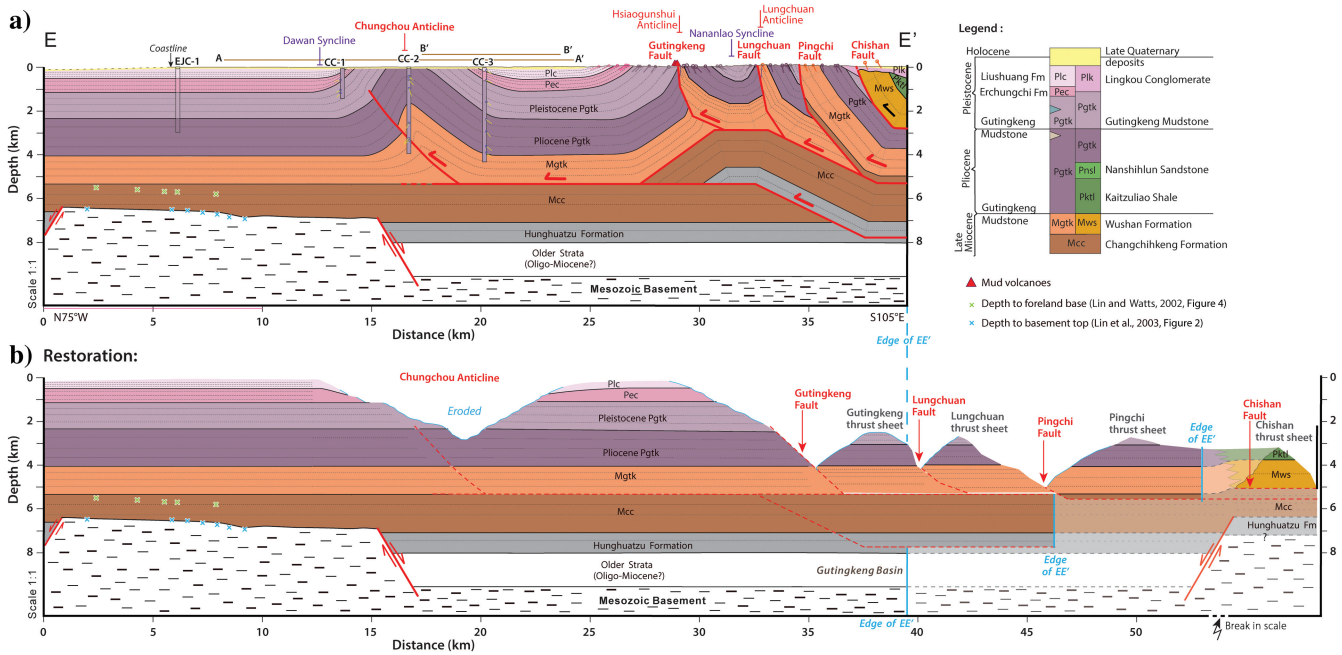

Figure 10. (a) Our subsurface interpretation along the geologic cross-section line EE′ (see the location in Figures 1 and 2). (b) Restoration of the cross section in (a).

In the actively deforming footwall of the Gutingkeng Fault, our geologic survey failed to find any fault that could explain the uplift of the western block relative to the eastern one (Figures 5, 7, and 8). Instead, the bedding is well preserved and consistent along the fault strike, with steep dips of 60°–80°WNW from the fault trace to approximately 2 km to the west. This suggests active folding as the cause of the uplift. Based on the cross-section EE′ (Figure 10a), it is proposed that the folding west of the Gutingkeng Fault occurs, on the one hand, due to the westward displacement of the forelimb of the deeper fault-bend fold. This process forms a 35°-west-dipping kink band and would lead to limited uplift up to 4–5 km west of the fault. On the other hand, the steeper dip domain close to the fault could have initiated as a footwall syncline during the propagation of the Gutingkeng thrust, and then, once the deformation front propagated westward, sustained compression could have led to the further shortening of the existing fold through flexure and layer thickening due to pure shear, facilitated by the weak rheology of the Gutingkeng mudstone. Meanwhile, the Gutingkeng thrust would have steepened and become harder to activate, possibly becoming inactive. This scenario could explain why the active uplift occurs mainly within the steep dip domain on the footwall and also extends slightly to the hanging wall. This mechanism is illustrated by an increase in the thickness of the mudstone sequence in the core of the footwall fold, as shown in Figure 10a.

The Chungchou Anticline involves a thick mudstone sequence in its core, with steep dips reported along borehole CC-2 in the central part of the fold. Based on the growth strata geometry (Figure 9), it may have developed as a fault-propagation fold, with pure shear within the basal strata and growing above a subhorizontal detachment located at a depth of approximately 5 km. The inferred relief of the fold, suggested by the steep dips, is quite large compared to the fold width, and the fold width is quite narrow compared to the detachment depth, which could hardly be shallower than 4.5–5.0 km, given the borehole dip data. Other structural models of detachment folds, including an asymmetry, could be proposed (e.g., Shaw et al., 2005; Brandes and Tanner, 2014). We note that these models would all require the presence of a less competent rock formation in the fold core.

Shortening and thrusting produce contractional structures in the presence of mobile shales, which are different from those produced in a classical fold-and-thrust belt (e.g., Mourgues et al., 2009; Morley et al., 2017; Dooley et al., 2024; Soto et al., 2024). We summarize, hereafter, the characteristics of our study area that are rather difficult to explain with classical thrust-related folding concepts and evoke shale tectonics, as schematically represented in Figure 11. Figure 11a shows fault-related folds commonly observed near the front of classical fold-and-thrust belts, with anticlines and synclines with a roughly similar width and shallow dipping limbs and uplift occurring above the thrust ramps (e.g., Shaw et al., 2005). In contrast, we observe narrow anticlines with steep limbs and a fold axis located very close to the thrust, along with much wider synclines (Figures 1 and 10a). Figure 11b has been designed with our cross-section EE′ in mind and depicts shale tectonics structures that could be encountered along our cross section while also incorporating other structures that typically appear to accompany mobile shales. For instance, duplexing appears to occur frequently within the shale sequences (no. 1 in Figure 11b) (Dooley et al., 2024). Shale tectonic processes could form narrow, high-relief anticlines through the inflation of shale sequences (here, the Gutingkeng mudstone) into the fold cores by the flow of weak, overpressured material. Shale mobilization could occur through plastic flow, withdrawing the mobile shales of the source layer in the synclines and inflating the near anticlines (no. 2 in Figure 11b), as well as infiltrating through the fault zones (no. 3 in Figure 11b), thereby creating mud volcanoes at the surface (Soto and Hudec, 2023). In the case of the Gutingkeng area mud volcanoes, the fluids would come from a shallower source (no. 4 in Figure 11b), possibly a part of the mobile shale sequence. Anticline inflation on the footwall of the thrusts causes the thrusts to steepen, in turn causing the back tilting of the hanging wall thrust sheets (no. 5 in Figure 11b). This could eventually lead to the inactivity of the thrust fault and the uplift occurring mainly due to the thickening of the footwall. Anticline inflation also leads to tighter anticlines near the crest of which, other structures, such as backthrusts, could develop (no. 6 in Figure 11b).

For the Chungchou and Gutingkeng structures, the pure-shear fault-related folding and mobile shale processes could provide solutions for the observed geometry of the structures and the active deformation patterns. Given the evidence for overpressure and the presence of mud volcanoes, we suggest that both mechanisms could have been occurring. This interpretation aligns with a comparable mud-involved fold at Liuchiu Island, located offshore southwestern Taiwan, which was proposed as a fault-related fold with the involvement of mobile shales by Wang et al. (2022). These authors supported their model using surface geology and offshore seismic reflection profiles, highlighting the asymmetry of growth strata. They found that the vertical deformation per unit shortening is 10 times larger for the Liuchiu Anticline compared with the Pakuashan Anticline in central Taiwan (Simoes et al., 2007), and the Yakeng and Anjihai Anticlines in the eastern Tien Shan area (Daëron et al., 2007), where the Neogene to the Quaternary sandstone and conglomerates predominate. Such a high order of vertical deformation could imply viscous or plastic deformation taking place within the mudstone layers, potentially due to the mobilization of shales under elevated pore-fluid pressures (Wang et al., 2022). In addition, because these mud-cored folds could be structurally continuous from offshore to onshore

(Sun and Liu, 1993; Huang, 1995; Chuang, 2006; Chen et al., 2020), it is plausible to interpret the Chungchou structure as a fault-related fold, possibly with the participation of mobile shales.

We have discussed processes potentially occurring along transect EE′. Mud volcanoes and rapid uplift have been observed elsewhere in the region as well. To the north of EE′, surface geology and leveling measurements (Figures 1 and 2) in the vicinity of the Lungchuan Fault (Le Béon et al., 2017) show characteristics similar to those in the Gutingkeng Fault area. The Lungchuan Fault trace is also associated with a series of mud volcanoes whose extruded materials share similar properties to those along the Gutingkeng Fault (Sun et al., 2010). Hence, shale tectonics could affect the footwall of the Lungchuan Fault in a way similar to the Gutingkeng Fault area. In contrast, to the south of EE′, a phenomenon with different characteristics was observed on the footwall of the Chishan Fault (Figure 1). There, geodesy reported local footwall uplift rates larger than the regional shortening rate, and structural observations documented normal faults along the edge of the uplift domain, with shale tectonics as the inferred cause (Ching et al., 2016; Chiou et al., 2019). In addition, mud volcanoes along the Chishan Fault expel deeper-sourced fluids (Sun et al., 2010). Additional work is necessary to propose an upper-crust structural model to explain the variety of phenomena observed in the region.

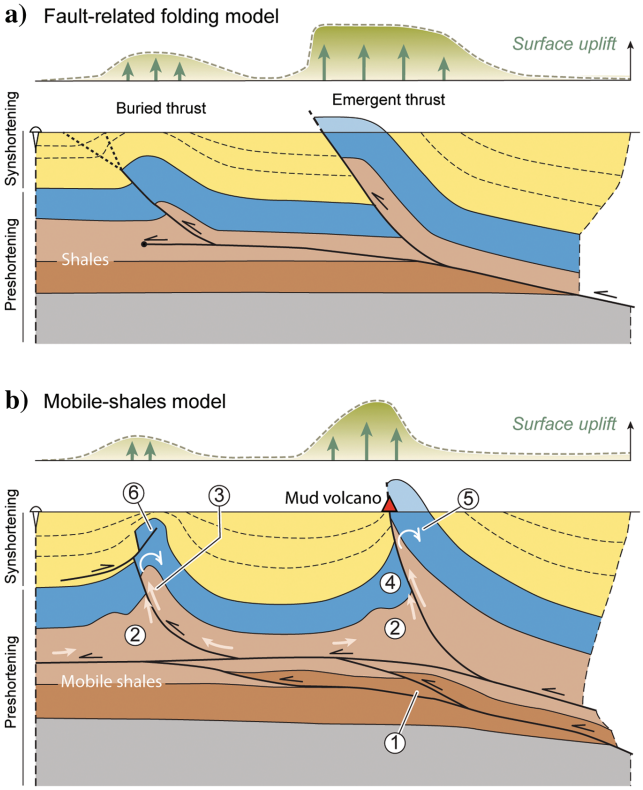

Figure 11. Schematic diagrams showing the characteristic structural features of a thrust system with syntectonic sedimentation. These diagrams summarize structural observations that can help differentiate between (a) a traditional thrust system model and (b) one involving mobile shales. Both diagrams include an idealized profile at the top, showing the variation in topographic uplift associated with the structures. (a) A conventional thrust system is depicted with a basal detachment located within a weak shale layer. (b) The numbered circles highlight key observations and structures typical of a mobile shale system under contraction. (1) Tectonic thickening through duplexing within the basal shale layer. (2) Shale thickening due to flow, inflating the thrust footwalls. (3) The flow of mobile shales in the footwall and hanging wall of thrusts and reverse faults, which may result in the formation of mud volcanoes at the surface. In the case of our transect EE′, shallow-sourced fluids would come from location (4). (5) Slip along high-angle reverse faults and footwall fold core inflation result in steepening (back rotation) of faults and hanging wall strata, possibly leading to fault inactivity. (6) The tightening of thrust-related anticlines, possibly leading to the formation of backthrusts.

Suggestions for further study

Whether a fold structure is primarily shaped by shale tectonics, fault-related folding, or a combination of both holds significant implications for the potential seismic risk associated with the structure. Fault-related folds are more commonly reported with seismic activity than mud diapirs (e.g., He et al., 2019; Wang et al., 2022). The extent of seismic and aseismic behaviors is contingent upon factors such as fluid contents (and, consequently, pore pressure), diagenetic history, and the degree of the compaction of the materials within the fault zone (e.g., Goulty et al., 2016; Morley et al., 2017). It is possible that deeper shales, having experienced drainage, tend to display stick-slip behaviors, whereas shallower shales, which remain undrained, could exhibit aseismic ductile deformation. It is crucial to emphasize that the seismic risk associated with mobile shale formations is a subject of ongoing research. The southwestern Taiwan fold-and-thrust belt stands out as an optimal natural setting for investigating this matter in the future, given its rapid shortening rates and relatively infrequent seismic events.

Understanding the possible role of mobile shales in creating the observed structures of the fold-and-thrust belt in southwestern Taiwan requires additional observations and further analysis. Additional studies in the region might help evaluate if a classical fold-and-thrust mechanism can explain the fold geometries and observed deformation entirely or if mobile shales are also required, in particular, to accommodate the increase in thickness that is inferred to occur in the subsurface at the core of the fault-related anticlines (Figure 10a). Although 3D seismic data currently appear to be key to the optimal imaging of structures involving shales (e.g., Wu et al., 2019; Soto and Hudec, 2023), such data are currently not available for Taiwan. Wang et al. (2022) show that the existing 2D seismic reflection data and their objective processing could prove instrumental in enhancing our knowledge of the subsurface structures off southwestern Taiwan. This approach, implemented on land, could provide valuable insights into the geometry of shale units in the coastal plain and foothills. In parallel, constraining geologic cross sections by

using the densities of the formations to reproduce the observed gravity anomalies can enhance the accuracy of structural interpretation. For example, understanding how positive and negative gravity anomalies vary over a mobile shale piercement structure and above a fold without mobile shale can provide valuable constraints on the distribution and geometry of subsurface structures. This integrated approach would provide a more comprehensive understanding of the deformation mechanisms in the study area, leading to more accurate geologic models and interpretations and aiding in the characterization of the possible role of mobile shales in the deformation processes.

Conclusion

Our study sheds light on the deformation structures in southwestern Taiwan, where the Late Miocene to Early Pleistocene Gutingkeng mudstone dominates the surface geology and has characteristics similar to mobile shales, including evidence of overpressured strata and the presence of mud volcanoes. Hence, it is crucial to consider mechanisms beyond classical fault-related folding, such as shale tectonics, in regional deformation. Through a combination of field investigation and subsurface data, we show that the deformation of the thick Gutingkeng mudstone plays a crucial role in accommodating orogenic shortening by thickening and folding. The Gutingkeng Fault zone displays penetrative brittle faulting in the mudstone series, characterized by steep, well-preserved bedding on hanging walls and footwalls and by mud volcanoes along the thrust. We interpret that the Gutingkeng Fault may be inactive, with uplift in the region primarily caused by folding and layer thickening within the footwall under the action of the westward displacement of the Gutingkeng thrust sheet toward the thick and weak mudstone on the footwall. Similarly, a fault-propagation fold with thickening of the weak basal strata was proposed for the Chungchou Anticline. In both structures, the weak rheology of the Gutingkeng mudstone could have been enhanced by the elevated pore-fluid pressure, which could have led to shale mobilization. Shale tectonics could be occurring in the core of the folds at depth, without clear evidence at the surface, aside from mud volcanism and increased surface uplift.

Findings from this study not only contribute to our understanding of the structural evolution of the region but also highlight the importance of weak mudstones in controlling the deformation pattern and style in this fold-and-thrust belt. This adds to ongoing efforts to understand the complex processes within active orogens involving mudstones and their implications for seismic hazards and ground surface displacement hazards in similar geologic settings worldwide. Using high-resolution seismic reflection data and gravity modeling of the anticlinal structures in southwestern Taiwan can enhance our comprehension of the subsurface structures. This approach will enable a clearer differentiation between the influences of shale tectonics and fault-related folding on deformation and the associated seismic hazard.

Acknowledgments

H. Aleem and M. Le Béon contributed equally to the research and writing of this paper. This paper benefitted from constructive reviews by D. Brown and two anonymous reviewers, as well as comments from editor C. Morley and associate editor D. Dunlap. This research was funded by the Taiwan National Science and Technology Council (NSTC) projects 111-2923-M-008-002-MY4 and 112-2116-M-008-007, led by M. Le Béon. In addition, J. I. Soto appreciates the support from the Applied Geodynamics Laboratory (AGL) Industrial Associates program. This publication is authorized by the Director of the Bureau of Economic Geology at The University of Texas at Austin.

Data and materials availability

Data associated with this research are available and can be obtained by contacting the corresponding author.

References

Alizadeh, A. A., I. S. Guliev, F. H. Dadashov, and R. R. Rahmanov, 2015, Atlas of the world mud volcanoes: Nafta Press, Azerbaijan National Academy of Sciences, Institute of Geology and Geophysics.

Álvarez-Marrón, J., D. Brown, G. Camanni, Y. M. Wu, and H. Kuo-Chen, 2014, Structural complexities in a foreland thrust belt inherited from the shelf-slope transition: Insights from the Alishan area of Taiwan: Tectonics, **33**, 1322–1339, doi: 10.1002/2014TC003584.

Biete, C., J. Álvarez-Marrón, D. Brown, and H. Kuo-Chen, 2018, The structure of southwest Taiwan: The development of a fold-and-thrust belt on a margin's outer shelf and slope: Tectonics, **37**, 1973–1993, doi: 10.1029/2017TC004910.

Bonini, M., 2007, Interrelations of mud volcanism, fluid venting, and thrust-anticline folding: Examples from the external northern Apennines (Emilia-Romagna, Italy): Journal of Geophysical Research: Solid Earth, **112**, B08413, doi: 10.1029/2006JB004859.

Brandes, C., and D. C. Tanner, 2014, Fault-related folding: A review of kinematic models and their application: Earth-Science Reviews, **138**, 352–370, doi: 10.1016/j.earscirev.2014.06.008.

Brown, D., J. Álvarez-Marrón, C. Biete, H. Kuo-Chen, G. Camanni, and C. W. Ho, 2017, How the structural architecture of the Eurasian continental margin affects the structure, seismicity, and topography of the south-central Taiwan fold and thrust belt: Tectonics, **36**, 1275–1294, doi: 10.1002/2017TC004475.

Brown, D., J. Álvarez-Marrón, G. Camanni, C. Biete, H. Kuo-Chen, and Y. M. Wu, 2022, Structure of the south-central Taiwan fold-and-thrust belt: Testing the viability of the model: Earth-Science Reviews, **231**, 104094, doi: 10.1016/j.earscirev.2022.104094.

Brown, K. M., 1990, The nature and hydrogeologic significance of mud diapirs and diatremes for accretionary systems: Journal of Geophysical Research: Solid Earth, **95**, 8969–8982, doi: 10.1029/JB095iB06p08969.

Camanni, G., J. Álvarez-Marrón, D. Brown, C. Ayala, Y. M. Wu, and H. H. Hsieh, 2016, The deep structure of south-central Taiwan illuminated by seismic tomography and earthquake hypocentre data: Tectonophysics, **679**, 235–245, doi: 10.1016/j.tecto.2015.09.016.

Casciello, E., M. Cesarano, and J. W. Cosgrove, 2004, Shear deformation of pelitic rocks in a large-scale natural fault, *in* G. I. Alsop, R. E. Holdsworth, K. J. W. McCaffrey, and M. Hand, eds., Flow processes in faults and shear zones: Geological Society, London, Special Publications 224, 113–125.

Castelltort, S., S. Nagel, F. Mouthereau, A. T. Lin, A. Wetzel, B. Kaus, S. Willett, S. P. Chiang, and W. Y. Chiu, 2011, Sedimentology of early Pliocene sandstones in the south-western Taiwan foreland: Implications for basin physiography in the early stages of collision: Journal of Asian Earth Sciences, **40**, 52–71, doi: 10.1016/j.jseaes.2010.09.005.

Chain, S., 1967, Study of pressure control in high pressure formation drilling: Petroleum Geology of Taiwan, **3**, 191–202.

Chao, H. C., C. F. You, H. C Liu, and C. H. Chung, 2013, The origin and migration of mud volcano fluids in Taiwan: Evidence from hydrogen, oxygen, and strontium isotopic compositions: Geochimica et Cosmochimica Acta, **114**, 29–51, doi: 10.1016/j.gca.2013.03.035.

Chao, H. C., C. F. You, and C. H. Sun, 2010, Gases in Taiwan mud volcanoes: Chemical composition, methane carbon isotopes, and gas fluxes: Applied Geochemistry, **25**, 428–436, doi: 10.1016/j.apgeochem.2009.12.009.

Chen, S. C., K.-E. Ching, Y.-T. Lo, and W.-C. Lu, 2020, Mud diapiric characters, activities, and geohazards of the Tainan and Chungchou anticlines: Journal of the Central Geological Survey, **33**, 1–32.

Chen, S. C., S. K. Hsu, Y. Wang, S. H. Chung, P. C. Chen, C. H. Tsai, C. H. Liu, H. S. Lin, and Y. W. Lee, 2014, Distribution and characteristics of mud diapirs and mud volcanoes off southwest Taiwan: Journal of Asian Earth Sciences, **92**, 201–214, doi: 10.1016/j.jseaes.2013.10.009.

Chen, Y. G., and T. K. Liu, 2000, Holocene uplift and subsidence along an active tectonic margin southwestern Taiwan: Quaternary Science Reviews, **19**, 923–930, doi: 10.1016/S0277-3791(99)00076-1.

Chi, W. R., 1978, The late Neogene nannobiostratigraphy in the Tainan foothills region, southern Taiwan: Petroleum Geology of Taiwan, **15**, 89–125.

Chi, W. R., 1979, A biostratigraphic study of the Late Neogene sediments in the Kaohsiung area based on calcareous nannofossils: Proceedings of the Geological Society of China, **22**, 121–144.

Chiang, S. C., 1971, Seismic study of the Chaochou structure, Pingtung, Taiwan: Petroleum Geology of Taiwan, **8**, 281–294.

Chinese Petroleum Corporation (CPC), 1989, Geological map of Tainan, scale 1:100,000: Petroleum Geology of Taiwan, Taiwan Petroleum Exploration Division, Chinese Petroleum Corporation, Republic of China.

Ching, K.-E., J. R. Gourley, Y.-H. Lee, S. C. Hsu, K. H. Chen, and C. L. Chen, 2016, Rapid deformation rates due to development of diapiric anticline in southwestern Taiwan from geodetic observations: Tectonophysics, **692**, 241–251, doi: 10.1016/j.tecto.2015.07.020.

Ching, K.-E., J.-C. Hu, H.-Y. Chen, W.-L. Chang, K.-C. Cheng, and Y.-R. Chuang, 2018, Monitoring of fault activity, Stage 4: Processing and analysis of surface deformation observations and fault model inversion (2/4) (in Chinese with English abstract): Report of the Central Geological Survey, Ministry of Economic Affairs, Taiwan.

Chiou, Y. W., Y.-C. Lin, W.-J. Huang, I.-C. Yen, M. Le Béon, and Y.-H. Lee, 2019, Characteristics of the Chishan Fault zone at northern entrance of the Zhongliao tunnel, southwest Taiwan: Special Publication of Central Geological Survey, **34**, 83–100.

Chiu, J.-K., T. Wei-Hao, and C.-S. Liu, 2006, Distribution of gassy sediments and mud volcanoes offshore southwestern Taiwan: Terrestrial, Atmospheric and Oceanic Sciences, **17**, 703, doi: 10.3319/TAO.2006.17.4.703(GH).

Chuang, H. J., 2006, Distribution and structural relationships of mud diapirs offshore southwestern Taiwan: M.S. thesis, National Taiwan University.

Cohen, H. A., and K. McClay, 1996, Sedimentation and shale tectonics of the northwestern Niger Delta front: Marine and Petroleum Geology, **13**, 313–328, doi: 10.1016/0264-8172(95)00067-4.

Covey, M., 1986, The evolution of foreland basins to steady state: Evidence from the western Taiwan foreland basin, *in* P. A. Allen and P. Homewood, eds., Foreland basins: John Wiley & Sons, 77–90.

Daëron, M., J.-P. Avouac, and J. Charreau, 2007, Modeling the shortening history of a fault tip fold using structural and geomorphic records of deformation: Journal of Geophysical Research: Solid Earth, **112**, B03S13, doi: 10.1029/2006JB004460.

Day-Stirrat, R. J., A. McDonnell, and L. J. Wood, 2010, Diagenetic and seismic concerns associated with interpretation of deeply buried mobile shales, *in* L. Wood, ed., Shale tectonics: AAPG Memoir 93, 5–27.

Doo, W.-B., S.-K. Hsu, C.-L. Lo, S.-C. Chen, C.-H. Tsai, J.-Y. Lin, Y.-F. Huang, Y.-S. Huang, S.-D. Chiu, and Y.-F. Ma, 2015, Gravity anomalies of the active mud diapirs off southwest Taiwan: Geophysical Journal International, **203**, 2089–2098, doi: 10.1093/gji/ggv430.

Dooley, T. P., J. I. Soto, J. E. Reber, M. R. Hudec, F. J. Peel, and G. M. Apps, 2024, Modeling mobile shales under

contraction: Critical analyses of new analog simulations of shale tectonics and comparison with salt-bearing systems: Interpretation, **12**, no. 4, SF17–SF38, doi: 10.1190/INT-2024-0025.1.

Fernández-Ibáñez, F., and J. I. Soto, 2017, Pore pressure and stress regime in a thick extensional basin with active shale diapirism (western Mediterranean): AAPG Bulletin, **101**, 233–264, doi: 10.1306/07131615228.

Fossen, H., 2016, Structural geology: Cambridge University Press.

Gong, S. Y., T. Y. Lee, J. C. Wu, S. W. Wang, and K. M. Yang, 1996, Possible links between the development of Plio-Pleistocene coral reef limestones and thrust migration in southwestern Taiwan: Journal of the Geological Society of China, **39**, 151–166.

Gong, S. Y., S. W. Wang, and T. Y. Lee, 1998, Pleistocene coral reefs associated with claystones, southwestern Taiwan: Coral Reefs, **17**, 215–222, doi: 10.1007/s003380050121.

Goulty, N. R., C. Sargent, P. Andras, and A. C. Aplin, 2016, Compaction of diagenetically altered mudstones — Part 1: Mechanical and chemical contributions: Marine and Petroleum Geology, **77**, 703–713, doi: 10.1016/j.marpetgeo.2016.07.015.

He, D., R. Lu, H. Huang, X. Wang, H. Jiang, and W. Zhang, 2019, Tectonic and geological setting of the earthquake hazards in the Changning shale gas development zone, Sichuan Basin, SW China: Petroleum Exploration and Development, **46**, 1051–1064, doi: 10.1016/S1876-3804(19)60262-4.

Ho, C. S., 1986, A synthesis of the geologic evolution of Taiwan: Tectonophysics, **125**, 1–16, doi: 10.1016/0040-1951(86)90004-1.

Horng, C. S., 2014, Age of the Tananwan formation in northern Taiwan: A reexamination of the magnetostratigraphy and calcareous nannofossil biostratigraphy: Terrestrial, Atmospheric and Oceanic Sciences, **25**, 137–147, doi: 10.3319/TAO.2013.11.05.01(TT).

Horng, C. S., and K. S. Shea, 1994, Study of nannofossil biostratigraphy in the eastern part of the Erhjen-chi section, southwestern Taiwan: Special Publication of Central Geological Survey, **8**, 181–204.

Hovland, M., A. Hill, and D. Stokes, 1997, The structure and geomorphology of the Dashgil mud volcano, Azerbaijan: Geomorphology, **21**, 1–15, doi: 10.1016/S0169-555X(97)00034-2.

Hsieh, M. L., and P. L. Knuepfer, 2001, Middle–late Holocene river terraces in the Erhjen River Basin, southwestern Taiwan — Implications of river response to climate change and active tectonic uplift: Geomorphology, **38**, 337–372, doi: 10.1016/S0169-555X(00)00105-7.

Hsieh, S. H., 1972, Subsurface geology and gravity anomalies of the Tainan and Chungchou structures of the Coastal Plain of southwestern Taiwan: Petroleum Geology of Taiwan, **10**, 323–338.

Hsu, Y. J., S. B. Yu, M. Simons, L. C. Kuo, and H. Y. Chen, 2009, Interseismic crustal deformation in the Taiwan plate boundary zone revealed by GPS observations, seismicity, and earthquake focal mechanisms: Tectonophysics, **479**, 4–18, doi: 10.1016/j.tecto.2008.11.016.

Huang, C.-C., 2015, Electron microscopic characterization and X-ray pole-figure diffraction of mudstones and fault gouges from northern Lungchuan Fault, Southern Taiwan (in Chinese with English abstract): M.S. thesis, National Cheng Kung University.

Huang, M. H., J. C. Hu, C. S. Hsieh, K.-E. Ching, R. J. Rau, E. Pathier, and B. Deffontaines, 2006, A growing structure near the deformation front in SW Taiwan as deduced from SAR interferometry and geodetic observation: Geophysical Research Letters, **33**, L12305, doi: 10.1029/2005GL025613.

Huang, M. H., H. Tung, E. J. Fielding, H. H. Huang, C. Liang, C. Huang, and J. C. Hu, 2016, Multiple fault slip triggered above the 2016 Mw 6.4 Meinong earthquake in Taiwan: Geophysical Research Letters, **43**, 7459–7467, doi: 10.1002/2016GL069351.

Huang, S. T., K. M. Yang, J. H. Hung, J. C. Wu, H. H. Ting, W. W. Mei, S. H. Hsu, and M. Lee, 2004, Deformation front development at the northeast margin of the Tainan basin, Tainan-Kaohsiung area, Taiwan: Marine Geophysical Researches, **25**, 139–156, doi: 10.1007/s11001-005-0739-z.

Huang, W. L., 1995, Distribution and mud diapirs offshore southwestern Taiwan, their relations to the onland anticlinal structures and their effects on the deposition environment in southwestern Taiwan: M.S. thesis, National Taiwan University.

Hudec, M. R., and J. I. Soto, 2021, Piercement mechanisms for mobile shales: Basin Research, **33**, 2862–2882, doi: 10.1111/bre.12586.

Jhuang, C.-J., 2023, Fault rocks and deformation mechanism of the Chegualin active fault in southwestern Taiwan (in Chinese with English abstract): M.S. thesis, National Central University.

Lacombe, O., J. Angelier, F. Mouthereau, H. T. Chu, B. Deffontaines, J. C. Lee, M. Rocher, R.F. Chen, and L. Siame, 2004, The Liuchiu Hsu island offshore SW Taiwan: Tectonic versus diapiric anticline development and comparisons with onshore structures: Comptes Rendus Geoscience, **336**, 815–825, doi: 10.1016/j.crte.2004.02.007.

Lacombe, O., F. Mouthereau, B. Deffontaines, J. Angelier, H. T. Chu, and C. T. Lee, 1999, Geometry and Quaternary kinematics of fold-and-thrust units of southwestern Taiwan: Tectonics, **18**, 1198–1223, doi: 10.1029/1999TC900036.

Le Béon, M., M. H. Huang, J. Suppe, S. T. Huang, E. Pathier, W. J. Huang, C. L. Chen, B. Fruneau, S. Baize, K.-E. Ching, and J. C. Hu, 2017, Shallow geological structures triggered during the Mw 6.4 Meinong earthquake, southwestern Taiwan: Terrestrial Atmospheric and Oceanic Sciences, **28**, 663–681, doi: 10.3319/TAO.2017.03.20.02.

Le Béon, M., O. Marc, J. Suppe, M. H. Huang, S. T. Huang, and W. S. Chen, 2019, Structure and deformation history

of the rapidly growing Tainan anticline at the deformation front of the Taiwan mountain belt: Tectonics, **38**, 3311–3334, doi: 10.1029/2019TC005510.

Lee, T. Y., C. H. Tang, J. S. Ting, and Y. Y. Hsu, 1993, Sequence stratigraphy of the Tainan Basin, offshore southwestern Taiwan: Petroleum Geology Taiwan, **28**, 119–158.

Lin, A. T., and A. B. Watts, 2002, Origin of the West Taiwan basin by orogenic loading and flexure of a rifted continental margin: Journal of Geophysical Research: Solid Earth, **107**, 2185, doi: 10.1029/2001JB000669.

Lin, A. T., A. B. Watts, and S. P. Hesselbo, 2003, Cenozoic stratigraphy and subsidence history of the South China Sea margin in the Taiwan region: Basin Research, **15**, 453–478, doi: 10.1046/j.1365-2117.2003.00215.x.

Lin, A. T. S., 2001, Cenozoic stratigraphy and tectonic development of the west Taiwan basins: Ph.D. thesis, University of Oxford.

Lin, C. W., C. J. Chiang, and P. J. Wu, 2013, Geological map of Qishan, scale 1:50,000, sheet 56: Central Geological Survey, Ministry of Economic Affairs.

Liu, C. C., J. S. Jean, B. Nath, M. K. Lee, L. I. Hor, K. H. Lin, and J. P Maity, 2009, Geochemical characteristics of the fluids and muds from two southern Taiwan mud volcanoes: Implications for water–sediment interaction and groundwater arsenic enrichment: Applied Geochemistry, **24**, 1793–1802, doi: 10.1016/j.apgeochem.2009.06.002.

Liu, C.-S., I. L. Huang, and L. S. Teng, 1997, Structural features off southwestern Taiwan: Marine Geology, **137**, 305–319, doi: 10.1016/S0025-3227(96)00093-X.

Lo, Y. T., K.-E. Ching, H. Y. Yen, and C. S. Chen, 2023, Bouguer gravity anomalies and the three-dimensional density structure of a thick mudstone area: A case study of southwestern Taiwan: Tectonophysics, **848**, 229730, doi: 10.1016/j.tecto.2023.229730.

Lu, C.-H., R. C. Chuang, P.-C. Chiang, J.-Y. Yen, K.-E. Ching, and Y.-G. Chen, 2024, Detecting infrastructure hazard potential change by SAR techniques on postseismic surface deformation: A case study of 2016 Meinong earthquake in southwestern Taiwan: Engineering Geology, **344**, 107827, doi: 10.1016/j.enggeo.2024.107827.

Mazzini, A., and G. Etiope, 2017, Mud volcanism: An updated review: Earth-Science Reviews, **168**, 81–112, doi: 10.1016/j.earscirev.2017.03.001.

Morley, C. K., 1992, Hydrocarbon generation — A possible cause of elevated pore pressures in the Osen-Roa thrust sheet, Norway: Journal of Structural Geology, **14**, 743–747, doi: 10.1016/0191-8141(92)90131-F.

Morley, C. K., 2003, Mobile shale-related deformation in large deltas developed on passive and active margins, *in* P. Van Rensbergen, R. R. Hillis, A. J. Maltman, and C. K. Morley, eds., Subsurface sediment mobilization: Geological Society of London, Special Publications 216, 335–357.

Morley, C. K., P. Crevello, and H. A. Zulkifli, 1998, Shale tectonics and deformation associated with active diapirism: The Jerudong Anticline: Journal of the Geological Society, **155**, 475–490, doi: 10.1144/gsjgs.155.3.0475.

Morley, C. K., and G. Guerin, 1996, Comparison of gravity driven deformation styles and behavior associated with mobile shales and salt: Tectonics, **15**, 1154–1170, doi: 10.1029/96TC01416.

Morley, C. K., R. King, R. Hillis, M. Tingay, and G. Backe, 2011, Deepwater fold and thrust belt classification, tectonics, structure and hydrocarbon prospectivity: A review: Earth-Science Reviews, **104**, 41–91, doi: 10.1016/j.earscirev.2010.09.010.

Morley, C. K., W. Promrak, W. Apuanram, P. Chaiyo, S. Chantraprasert, D. Ong, A. Suphawajruksakul, N. Thaemsiri, and M. Tingay, 2023, A major Miocene deepwater mud canopy system: The North Sabah–Pagasa Wedge, northwestern Borneo: Geosphere, **19**, 291–334, doi: 10.1130/GES02518.1.

Morley, C. K., C. von Hagke, R. L. Hansberry, A. S. Collins, W. Kanitpanyacharoen, and R. King, 2017, Review of major shale-dominated detachment and thrust characteristics in the diagenetic zone: Part I, meso- and macro-scopic scale: Earth-Science Reviews, **173**, 168–228, doi: 10.1016/j.earscirev.2017.07.019.

Morley, C. K., C. von Hagke, R. L. Hansberry, A. S. Collins, W. Kanitpanyacharoen, and R. King, 2018, Review of major shale-dominated detachment and thrust characteristics in the diagenetic zone: Part II, rock mechanics and microscopic scale: Earth-Science Reviews, **176**, 19–50, doi: 10.1016/j.earscirev.2017.09.015.

Morley, C. K., J. Warren, M. Tingay, P. Boonyasaknanon, and A. Julapour, 2014, Comparison of modern fluid distribution, pressure and flow in sediments associated with anticlines growing in deepwater (Brunei) and continental environments (Iran): Marine and Petroleum Geology, **51**, 210–229, doi: 10.1016/j.marpetgeo.2013.11.011.

Mourgues, R., E. Lecomte, B. Vendeville, and S. Raillard, 2009: An experimental investigation of gravity-driven shale tectonics in progradational delta: Tectonophysics, **474**, 643–656, doi: 10.1016/j.tecto.2009.05.003.

Mouthereau, F., O. Lacombe, B. Deffontaines, J. Angelier, and S. Brusset, 2001, Deformation history of the southwestern Taiwan foreland thrust belt: Insights from tectono-sedimentary analyses and balanced cross-sections: Tectonophysics, **333**, 293–322, doi: 10.1016/S0040-1951(00)00280-8.

Mouthereau, F., O. Lacombe, and B. Meyer, 2006, The Zagros folded belt (Fars, Iran): Constraints from topography and critical wedge modelling: Geophysical Journal International, **165**, 336–356, doi: 10.1111/j.1365-246X.2006.02855.x.

Nagel, S., S. Castelltort, A. Wetzel, S. Willett, F. Mouthereau, and A. T. Lin, 2013, Sedimentology and foreland basin paleogeography during Taiwan arc continent collision: Journal of Asian Earth Sciences, **62**, 180–204, doi: 10.1016/j.jseaes.2012.09.001.

Oinomikado, T., 1955, Micropalaeontological Investigation of the Chishan Standard Section, near Tainan, Taiwan, China: Chinese Petroleum Company Palaeontology Laboratory Report, 7–10.

Pan, Y. S., 1968, Interpretation and seismic coordination of the Bouguer gravity anomalies obtained in southwestern Taiwan: Petroleum Geology of Taiwan, **6**, 197–208.

Pathier, E., B. Fruneau, M. P. Doin, Y. T. Liao, J. C. Hu, and J. Champenois, 2014, What are the tectonic structures accommodating the present-day tectonic deformation in South-Western Taiwan? A new interpretation from ALOS-1 InSAR and GPS interseismic measurements: 7th France-Taiwan Earth Sciences Symposium on Geodynamics and Environment in East-Asia.

Poblet, J., 2011, 2D kinematic models of growth fault-related folds in contractional settings, *in* C. Busby and A. A. Pérez, eds., Tectonics of sedimentary basins: Recent advances: Blackwell 27, 538–564.

Poblet, J., and K. McClay, 1996, Geometry and kinematics of single-layer detachment folds: AAPG Bulletin, **80**, 1085–1109, doi: 10.1306/64ED8CA0-1724-11D7-8645000102C1865D.

Sandal, S. T., 1996, The geology and hydrocarbon resources of Negara Brunei Darussalam: Syabas Publishers.

Shaw, J. H., C. Connors, and J. Suppe, eds., 2005, Seismic interpretation of contractional fault-related folds: AAPG, Studies in Geology 53.

Shi, R.-C., W.-H. Wang, and Y.-H. Lee, 2008, Earthquake geology and earthquake hazard assessment: Investigation of subsurface structure of fault zones (2/4) (in Chinese with English abstract): Report of the Central Geological Survey, Ministry of Economic Affairs, Taiwan, Nb. 97–11.

Shyu, J. B. H., Y. R. Chuang, Y. L. Chen, Y. R. Lee, and C. T. Cheng, 2016, A new on-land seismogenic structure source database from the Taiwan earthquake model (TEM) project for seismic hazard analysis of Taiwan: Terrestrial, Atmospheric and Oceanic Sciences, **27**, 311–323, doi: 10.3319/TAO.2015.11.27.02(TEM).

Simoes, M., J. P. Avouac, Y.-G. Chen, A. K. Singhvi, C.-Y. Wang, and M. Jaiswal, 2007, Kinematic analysis of the Pakuashan fault tip fold, west central Taiwan: Shortening rate and age of folding inception: Journal of Geophysical Research: Solid Earth, **112**, B03S14, doi: 10.1029/2005JB004198.

Skeryanc, A. J., and C. R. Kolodny, 1983, Syndepositional structures on mobile substrates, *in* A. W. Bally, ed., Seismic expression of structural styles: AAPG, Studies in Geology Series 15, 2.3.1-41–2.3.142.

Soto, J. I., T. P. Dooley, M. R. Hudec, F. J. Peel, and G. M. Apps, 2024, Shortening a mixed salt and mobile shale system: A case study from East Breaks, NW Gulf of Mexico: Interpretation, **12**, no. 4, SF77–SF103, doi: 10.1190/INT-2024-0049.1.

Soto, J. I., F. Fernández-Ibáñez, A. R. Talukder, and P. Martínez-García, 2010, Miocene shale tectonics in the northern Alboran Sea (western Mediterranean), *in* L. Wood, ed., Shale tectonics: AAPG Memoir 93, 119–144.

Soto, J. I., M. Heidari, and M. R. Hudec, 2021a, Proposal for a mechanical model of mobile shales: Scientific Reports, **11**, 23785, doi: 10.1038/s41598-021-02868-x.

Soto, J. I., and M. R. Hudec, 2023, Mud volcanoes guided by thrusting in compressional settings: Geology, **51**, 779–784, doi: 10.1130/G51235.1.

Soto, J. I., M. R. Hudec, N. H. Mondol, and M. Heidari, 2021b, Shale transformations and physical properties — Implications for seismic expression of mobile shales: Earth-Science Reviews, **220**, 103746, doi: 10.1016/j.earscirev.2021.103746.

Sun, C. H., S. C. Chang, C. L. Kuo, J. C. Wu, P. H. Shao, and J. N. Oung, 2010, Origins of Taiwan's mud volcanoes: Evidence from geochemistry: Journal of Asian Earth Sciences, **37**, 105-116, doi: 10.1016/j.jseaes.2009.02.007.

Sun, S. C., and C.-S. Liu, 1993, Mud diapirs and submarine channel deposits in offshore Kaohsiung-Hengchun, southwest Taiwan: Petroleum Geology of Taiwan, **28**, 1–14.

Suppe, J., 1980, Imbricated structure of western foothills belt, south-central Taiwan: Petroleum Geology of Taiwan, **17**, 1–16.

Suppe, J., 1981, Mechanics of mountain-building and metamorphism in Taiwan: Memoir of Geological Society of China, **4**, 67–89.

Suppe, J., 1986, Reactivated normal faults in the western Taiwan fold-and-thrust belt: Memoir of the Geological Society of China, **7**, 187–200.

Suppe, J., and Y. L. Chang, 1983, Kink method applied to structural interpretation of seismic sections, Western Taiwan: Petroleum Geology of Taiwan, **19**, 29–49.

Taylor, B., and D. E. Hayes, 1983, Origin and history of the South China Sea basin, *in* D. E. Hayes, ed., The tectonic and geologic evolution of Southeast Asian seas and islands: Part 2: American Geophysical Union Geophysical, AGU Monograph Series 27, 23–56.

Teng, L. S., 1990, Geotectonic evolution of late Cenozoic arc-continent collision in Taiwan: Tectonophysics, **183**, 57–76, doi: 10.1016/0040-1951(90)90188-E.

Teng, L. S., and A. T. Lin, 2004, Cenozoic tectonics of the China continental margin: Insights from Taiwan, *in* J. Malpas, C. J. N. Fletcher, J. R. Ali, and J. C. Aitchison, eds., Aspects of the tectonic evolution of China: Geological Society of London, Special Publications 226, 313–332.

Tingay, M. R. P., 2017, Initial pore pressures under the Lusi mud volcano, Indonesia: Interpretation, **3**, no. 1, SE33–SE49, doi: 10.1190/INT-2014-0092.1.

Tingay, M. R. P., R. R. Hillis, R. E. Swarbrick, C. K. Morley, and A. R. Damit, 2007, "Vertically transferred" overpressures in Brunei: Evidence for a new mechanism for the formation of high-magnitude overpressure: Geology, **35**, 1023–1026, doi: 10.1130/G23906A.1.

Tingay, M. R. P., R. R. Hillis, R. E. Swarbrick, C. K. Morley, and A. R. Damit, 2009, Origin of overpressure and

pore-pressure prediction in the Baram province, Brunei: AAPG Bulletin, **93**, 51–74, doi: 10.1306/08080808016.

Tingay, M. R. P., C. K. Morley, A. Laird, O. Limpornpipat, K. Krisadasima, S. Pabchanda, and H. R. Macintyre, 2013, Evidence for overpressure generation by kerogen-to-gas maturation in the northern Malay Basin: AAPG Bulletin, **97**, 639–672, doi: 10.1306/09041212032.

Vendeville, B. C., and M. P. A. Jackson, 1992, The rise of diapirs during thin-skinned extension: Marine and Petroleum Geology, **9**, 331–354, doi: 10.1016/0264-8172(92)90047-I.

Vrolijk, P., and B. A. Van der Pluijm, 1999, Clay gouge: Journal of Structural Geology, **21**, 1039–1048, doi: 10.1016/S0191-8141(99)00103-0.

Wang, Y., Y. N. Lin, Y. Ota, L. H. Chung, J. B. H. Shyu, H. W. Chiang, Y. G. Chen, H.-H. Hsu, and C. C. Shen, 2022, Mud diapir or fault-related fold? On the development of an active mud-cored anticline offshore Southwestern Taiwan: Tectonics, **36**, e2022TC00723, doi: 10.1029/2022TC007234.

Wood, L. J., 2010, Shale tectonics: A preface, *in* L. Wood, ed., Shale tectonics: AAPG Memoir 93, 1–4.

Wu, J., K. McClay, and J. de Vera, 2019, Growth of triangle zone fold-thrusts within the NW Borneo deep-water fold belt, offshore Sabah, southern South China Sea: Geosphere, **16**, 329–356, doi: 10.1130/GES02106.1.

Yang, K.-M., S.-T. Huang, J.-C. Wu, H.-H. Ting, and W.-W. Mei, 2006, Review and new insights on foreland tectonics in western Taiwan: International Geology Review, **48**, 910–941, doi: 10.2747/0020-6814.48.10.910.

Yang, K.-M., R.-J. Rau, H.-Y. Chang, C.-Y. Hsieh, H.-H. Ting, S.-T. Huang, J.-C. Wu, and Y.-J. Tang, 2016, The role of basement-involved normal faults in the recent tectonics of western Taiwan: Geological Magazine, **153**, 1166–1191, doi: 10.1017/S0016756816000637.

Yang, T. N., C. H. Hsu, C. C. Yang, P. N. Li, and M. J. Liu, 2018, Biostratigraphic study of the Upper Miocene to Pliocene Calcareous Nannofossils in the Foothill Belt of Southwestern Taiwan: 107th Joint Annual Meeting of the Geological Society of Taiwan and the Geophysical Society of the Republic of China.

Yi, D. C., R. Y. Chuang, L. H. Chung, C. W. Lin, and R. J. Rau, 2023, Surface deformation induced by the 2016 Meinong earthquake and its implications to active folds: Terrestrial, Atmospheric and Oceanic Sciences, **34**, 21, doi: 10.1007/s44195-023-00053-3.

You, C. F., J. M. Gieskes, T. Lee, T. F. Yui, and H. W. Chen, 2004, Geochemistry of mud volcano fluids in the Taiwan accretionary prism: Applied Geochemistry, **19**, 695–707, doi: 10.1016/j.apgeochem.2003.10.004.

Yuan, J., S.-T. Huang, T.-F. Chou, J.-C. Wu, and D.-L. Lu, 1987, The origin of the abnormal pressure zones in Southwestern Taiwan: Annual Exploration and Production (CPC), **10**, 1–27.

Yue, L. F., and J. Suppe, 2014, Regional pore-fluid pressures in the active western Taiwan thrust belt: A test of the classic Hubbert–Rubey fault-weakening hypothesis: Journal of Structural Geology, **69**, 493–518, doi: 10.1016/j.jsg.2014.08.002.

Biographies and photographs of the authors are not available.